Title
Sensor Analytics for Healthcare Improvement

Author
Huang, Ming-Chun

Publication Date
2014

Peer reviewed|Thesis/dissertation

University of California
Los Angeles

Sensor Analytics for Healthcare Improvement

A dissertation submitted in partial satisfaction
of the requirements for the degree
Doctor of Philosophy in Computer Science

by

Ming-Chun Huang

2014

Abstract of the Dissertation

Sensor Analytics for Healthcare Improvement

by

Ming-Chun Huang

Doctor of Philosophy in Computer Science

University of California, Los Angeles, 2014

Professor Majid Sarrafzadeh, Chair

The increasing proportion of older adults and corresponding costs associated with chronic disease management demand novel technological solutions. It is expected that new healthcare services will shift from clinical and hospital settings to a personalized and homebound environment. Along with the rapid advances in several technological domains including sensing, communication, and human factors design in the last decade, new technologies have led to the development of new mobile and personalized systems capable of analyzing and visualizing varying heterogeneous physiological signals. This dissertation presents an end-to-end research methodology for design and development of next generation wireless health applications, with a particular emphasis on innovative sensing systems design.

I summarize my research in wireless health domain: from On-bed physiological signals monitoring, Contactless vital signs monitoring, Augmented visualization, Virtual reality based rehabilitation, to Social activity promotion. Each project involved medical problem identification, feasible solution development, and clinical verification. In this dissertation, I address novel hardware and software sensing and interaction technologies, including sensor system design, sensor modeling, and sensor signal processing. The ultimate goals of this interdisciplinary research are to support our medical hypothesis, verify the feasibility of technological solutions in clinics, and eventually enable wireless health from concept to practice.

The dissertation of Ming-Chun Huang is approved.

Barbara Bates-Jensen

Lixia Zhang

Mario Gerla

Majid Sarrafzadeh, Committee Chair

University of California, Los Angeles

2014

To my beloved family and friends.

Table of Contents

List of Figures

List of Tables

Acknowledgments

I would like to sincerely thank my advisor, Professor Majid Sarrafzadeh. I was fortunate and honored to work under his supervision. He shared with me his knowledge and brilliant ideas, along with his friendliness and sense of humor throughout the entire dissertation constructing process. His thoughts and guidance, stemming from his experience and vision in Wireless Health research, cultivated me with fruitful ideas and innovations. His diligence, passion, and preciseness in research, deeply influenced my research attitude and future direction.

I would also like to express my gratitude to my Ph.D. committee members, Professor Mario Gerla, Professor Lixia Zhang, and Professor Barbara Bates-Jensen, for their guidance, insightful comments, and feedback towards my research path. I also appreciate Professor Jeff Burke for his thoughtful suggestions and assistance in my qualifying exam preparation.

Besides, I want thank my labmates, Wenyao Xu, Jason J. Liu, Nabil Alshurafa, Mars Lan, Hassan Ghasemzadeh, Mahsan Rofouei, Navid Amini, Bobak J. Razavi, Sunghoon I. Lee, Tannaz Tehrani, and Xiaoyi Zhang, for sharing their ideas and useful tools with me. It is an unforgotten experience to work with them.

Lastly, I want to sincerely thank my parents, Jiann-Tsuen Hwang and Hui-Tzu Peng, for their endless giving and loving. I would also like to give my greatest thanks to Yi Su and Tzu-Han Huang for keeping me company to the end. Their support and love make my dream come true. I am forever grateful to have them be a part of my life.

Vita

2007 B.S. (Electrical Engineering), National Tsing Hua University, Taiwan.

2010 M.S. (Electrical Engineering), University of Southern California, United States.

Publications

Jason J. Liu, **Ming-Chun Huang**, Wenyao Xu, Xiaoyi Zhang, Luke Steven, Nabil Alshurafa, and Majid Sarrafzadeh, "*BreathSens: A Continuous On-Bed Respiratory Monitoring System with Torso Localization using an Unobtrusive Pressure Sensing Array*", Journal of Biomedical and Health Informatics (**J-BHI**)

Ming-Chun Huang, Jason J. Liu, Wenyao Xu, Nabil Alshurafa, and Majid Sarrafzadeh, "*Using Pressure Map Sequences for Recognition of On Bed Rehabilitation Exercises*", Journal of Biomedical and Health Informatics (**J-BHI**), vol 18, num 2, Pages 411 - 418.

Ming-Chun Huang, Si-Huei Lee, Shih-Ching Yeh, Rai-Chi Chan, Albert Rizzo, and Wenyao Xu, "*Intelligent Frozen Shoulder Rehabilitation*", IEEE Intelligent Systems (**IS**).

Peter B. Lillehoj, **Ming-Chun Huang**, Newton Truong, and Chih-Ming Ho, "*Rapid electrochemical detection on a mobile phone*", **Lab on a Chip**, vol. 13, Pages 2950 - 2955.

Shih-Ching Yeh, **Ming-Chun Huang**, Pa-Chun Wang, Te-Yung Fang, Mu-Chun Su, Po-Yi Tsai, and Albert Rizzo, "*Machine Learning-based Assessment Tool for Imbalance and Vestibular Dysfunction with Virtual Reality Rehabilitation System*", Computer Methods and Programs in Biomedicine (**CMPB**).

Wenyao Xu, **Ming-Chun Huang**, Navid Amini, Lei He, and Majid Sarrafzadeh, "*eCushion: A Textile Pressure Sensor Array Design and Calibration for Sitting Posture Analysis*", IEEE Sensors Journal (**SJ**), Volume 13, Number 10, 2013, Pages 3926 - 3924.

Lauren Samy, **Ming-Chun Huang**, Jason J. Liu, Wenayo Xu, Xiaoyi Zhang, and Majid Sarrafzadeh, "*Unobtrusive Sleep Stage Identification Using a Pressure Sensitive Bed Sheet"*, IEEE Sensors Journal (**SJ**).

Jason J. Liu, **Ming-Chun Huang**, Wenyao Xu, Nabil Alshurafa, Majid Sarrafzadeh, Nitin Raut, and Behrooz Yadegar, "*Sleep Posture Analysis using using a Dense Pressure Sensitive Bedsheet*", Pervasive and Mobile Computing Journal (**PMC**).

Nabil Alshurafa, Wenyao Xu, Jason J. Liu, **Ming-Chun Huang**, Bobak Mortazavi Christian K. Roberts, and Majid Sarrafzadeh, "*Designing a Robust Activity Recognition Framework for Health and Exergaming using Wearable Sensors*", Journal of Biomedical and Health Informatics (**J-BHI**).

Jason J. Liu, **Ming-Chun Huang**, Wenyao Xu, and Majid Sarrafzadeh, "*Body-part Localization for Pressure Ulcer Prevention*", Conference of the IEEE Engineering in Medicine and Biology Society (**EMBC'14**), Chicago, USA, August 2014.

Ming-Chun Huang, Wenyao Xu, Xiaoyi Zhang, Jason J. Liu, and Majid Sarrafzadeh, "*EZwakeup: a sleep environment design for sleep quality improvement*", Conference on Human Factors in Computing Systems (**CHI'14**), Toronto, Canada, May 2014.

Ming-Chun Huang, Wenyao Xu, Jason Liu, Lei He and Majid Sarrafzadeh, "*Inconspicuous Personal Computer Protection with Touch-Mouse*", International Conference on Human Computer Interaction (**HCI'13**), Las Vegas, Nevada, USA, July 2013.

Jason Liu, Wenyao Xu, **Ming-Chun Huang**, Nabil Alshurafa and Majid Sarrafzadeh, "*A Dense Pressure Sensitive Bedsheet Design for Unobtrusive Sleep Posture Monitoring*", IEEE International Conference on Pervasive Computing and Communication (**PerCom'13**), San Diego, CA, USA, March 2013.

Peter. B. Lillehoj, **Ming-Chun Huang**, and Chih-Ming Ho, "*A Handheld Cell Phone-Based Electrochemical Biodetector*", Proc. of 26th **IEEE MEMS'13**.

Ming-Chun Huang, Shuya Chen, Pa-Chun Wang, Mu-Chun Su, Yen-Po Hung, Chia-Huang Chang, and Shih-Ching Yeh, "*Automate Virtual Reality Rehabilitation Evaluation for Chronic Imbalance and Vestibular Dysfunction Patients*", Advanced Technologies, Embedded and Multimedia for Human-centric Computing (**EMC'13**), Taipei, Taiwan, August 2013.

Xiaoyi Zhang, **Ming-Chun Huang**, Fengbo Ren, Wenyao Xu, Nan Guan, and Wang Yi, "*Proper Running Posture Guide: Wearable Biomechanics Capture System*", 8th International Conference on Body Area Networks (**BodyNet'13**), Boston, USA, October 2013.

Xiaoyi Zhang, Wenyao Xu, **Ming-Chun Huang**, Navid Amini, and Fengbo Ren, "*See UV on Your Skin: An Ultraviolet Sensing and Visualization System*", 8th International Conference on Body Area Networks (**BodyNet'13**), Boston, USA, October 2013.

Wenyao Xu, **Ming-Chun Huang**, Jason J. Liu, Fengbo Ren, Xinchen Shen, Xiao Liu and Majid Sarrafzadeh, "*Microphone-based Spirometer for COPD*", International Conference on Pervasive Technologies Related to Assistive Environments (**PETRA'13**), Rhodes Island, Greece, May 2013.

Ming-Chun Huang, Wenyao Xu, Jason Liu, Lauren Samy and Majid Sarrafzadeh, "*Smart Bedsheet Design for Non-invasive Respiration Rate Measurement*", International Conference on Pervasive Technologies Related to Assistive Environments (**PETRA'13**), Rhodes Island, Greece, May 2013.

Jason J. Liu, **Ming-Chun Huang**, Wenyao Xu, Nabil Alshurafa, Majid Sarrafzadeh, "*On-bed Monitoring for Range of Motion Exercises with a Pressure Sensitive Bedsheet*", IEEE International Conference on Implantable and Wearable Body Sensor Networks (**BSN'13**), Boston, MA, May 2013.

Nabil Alshurafa, Wenyao Xu, Jason J. Liu, **Ming-Chun Huang**, Bobak Mortazavi, Christian Roberts, Majid Sarrafzadeh, "*Robust Human Intensity-Varying Activity Recognition using Stochastic Approximation in Wearable Sensors*", IEEE International Conference on Implantable and Wearable Body Sensor Networks (**BSN'13**), Boston, MA, May 2013.

Ming-Chun Huang, Wenyao Xu, Chien-Yen Chang, Belinda Lange, Yi Su and Majid Sarrafzadeh, "*Smart Glove for Upper Extremities Rehabilitative Gam-*

ing Assessment", International Conference on Pervasive Technologies Related to Assistive Environments (**PETRA'12**), Crete Island, Greece, June 2012.

Wenyao Xu, **Ming-Chun Huang**, Navid Amini, Jason Liu, Lei He and Majid Sarrafzadeh, "*SmartInsole: A Wearable System for Gait Analysis*", International Conference on Pervasive Technologies Related to Assistive Environments (**PETRA'12**), Crete Island, Greece, June 2012.

Ming-Chun Huang, Ethan Chen, Wenyao Xu, Majid Sarrafzadeh, Belinda Lange, Chein-Yen Chang, "*Gaming for Upper Extremities Rehabilitation*", ACM Conference on Wireless Health (**WH'11**), San Diego, CA, October 2011.

Navid Amini, Wenyao Xu, Zhinan Li, **Ming-Chun Huang**, Majid Sarrafzadeh, "*Experimental Analysis of IEEE 802.15.4 for On/Off Body Communications*", IEEE Symposium on Personal Indoor Mobile Radio Communications (**PIMRC'11**), Toronto, Canada, September 2011.

Wenyao Xu, Zhinan Li, **Ming-Chun Huang**, Navid Amini, Majid Sarrafzadeh, "*eCushion: An eTextile Device for Sitting Posture Analysis*", IEEE Conference on Body Sensor Networks (**BSN'11**), Dallas, TX, May 2011.

CHAPTER 1

Introduction

To better incorporate science and technology into our lives, researchers are eager to understand human natural behaviors interacting with devices used daily. By understanding the interaction between human behaviors and devices, we can design better human-computer interfaces to facilitate and enrich our daily lives. However, it is not trivial to design a system to continuously record natural human behaviors without interrupting people's daily activities. Incautious designs may result in mental or physical behavioral changes of the users. This dissertation explores the feasibility of designing sensing and recording systems for On-bed physiological signals monitoring, Contactless vital signs monitoring, Augmented visualization, Virtual reality based rehabilitation, and Social activity promotion. Due to the fact that the system is embedded in devices we are familiar with, it is natural to retrieve collected human behaviors and interchange information with the name of the devices we used daily. Each sensing and recording unit should be able to securely share collected behavioral data with others in a distributed manner via a hierarchical naming structure.

I summarize the progress on my five wireless health research. As part of my research vision, I have identified and developed many novel, cost effective, deployable, and application-specific medical sensing systems. They can be easily used in daily life by exploring, designing and building advanced sensors and signal processing technologies.

In Chapter 2, I present an on-bed motion monitoring system, which consists

of a high density pressure-sensitive bedsheet and a sequence of methods to detect sleep postures, movements, calculate pressure accumulation, and extract physiological information. In contrast to existing techniques, our bedsheet system offers completely unobtrusive methods to detect on-bed motion by using comfortable textile materials. We developed a novel framework for pressure image analysis and ran a pilot study to evaluate the performance of our methods with 12 subjects, based on the high-resolution pressure data collected from the bedsheet system. Our experiment results revealed that our proposed method enables reliable sleep posture recognition and pressure accumulation calculation. In addition, the proposed system has the potential to monitor human movement and respiration without extra instruments involved. Physiological signals can be non-invasively extracted by analyzing time-stamped pressure distribution sequences. This is important information required in many clinical applications, including detection and monitoring of sleep disorders, monitoring of newborns for Sudden Infant Death Syndrome (SIDS), and identifying patients at high risk up to 24 hours before an adverse event like stroke and cardiac arrest. Failing to perform continuous and quantified measurements could result in an inability to rescue a patient exhibiting respiratory distress. Severe after effects hinder recovery, result in loss of time, cost, and even life. The proposed bedsheet system provides a 24/7 quantified on-bed movement and physiological signals monitoring service. It is made of textile and is similar to the regular bedsheet in comfort. As a result, it can seamlessly fit in common clinic or home environment, reducing the possible interference to a patient's regular sleeping habits.

In Chapter 3, I present a noncontact, self-calibrating vital sign monitoring system that comprises four layers based on Doppler radar. A framework was proposed to automatically analyze $I(t)/Q(t)$ signals collected from the radar sensor, including direct signal modeling, model parameter identification, and demodulation. Signal model identification was formulated into a quadratically constrained

ℓ_1 minimization problem and solved using upper bound and LMI relaxation. Three sets of experiments were conducted to evaluate the performance of the system. The accuracy and stability of the proposed demodulation framework was demonstrated and the end-to-end performance was examined using real-life scenarios. The results indicated that our system can effectively measure human vital signs without calibrating for each subject and distinct external environment.

In Chapter 4, I describe the design, implementation, and evaluation of our Ultra Violet(UV) monitoring and visualization system to effectively warn users to take protection and avoid possible sunburn beforehand. Four skin models help us estimate damaging UV dose for an individual person. According to the UV dose, our visualization system can provide a warning to the user beforehand by over-amplified sunburn visual effect on the user's arm. During the experiment, our participants gave very positive feedback on the visualization effect.

In Chapter 5, I introduce an innovative frozen shoulder rehabilitation system which is developed for the rehabilitation training of the patients shoulder Range of Motion(ROM) and muscular endurance. This study successfully conducted RCT clinical trials with 32 patients. While the feasibility of this system is demonstrated, its rehabilitation effectiveness towards frozen shoulders has also been verified. It was proven that it exhibited a rehabilitation effectiveness that was superior to that of the conventional rehabilitation exercises. The technology acceptance was identified from user perspective, indicating that participants were highly engaged with game-like tasks and had strong intention to continue the use of the proposed system for rehabilitation.

In Chapter 6, FridgeNet is introduced for older adults to share their diet information, food suggestions, and comments with other participants and their families. It provided a convenient social platform to exchange diet information and provide novel social services to promote older adults social activities. The findings reveal that sharing personal diet habits can be an attractive social topic

among older adults. FridgeNet effectively motivated older adults to share their knowledge, to communicate, and to meet with their peers virtually and physically. Both virtual and physical social activities increased during the 12-week study period. A virtual community was established and a group of shoppers formed during the study period. It was also reported that elderly participants possessed a more positive attitude and felt healthier after using FridgeNet than before.

CHAPTER 2

On-bed Physiological Signals Monitoring

2.1 Introduction

Urgent medical care is required when patients have abnormal respiration such as tachypnea (high respiration), bradypnea (low respiration), or apnea (no respiration). Peberdy et al. reported that 44% of over 14,000 cardiac arrests in acute care hospitals were attributed to respiratory problems [PKO03]. Furthermore, the 2011 HealthGrades study showed that 20% of post-operative respiratory failures in 5000 hospitals resulted in death [RM11]. Hodgetts et al. [HKV02] and Fieselmann et al. [FHH93] observed a large proportion of cardiac arrest patients had high respiration rate. In addition, the variation in respiratory rate is another important marker for cardiac arrest or admission to the intensive care unit [CCH07a].

Despite such information, respiration rate monitoring has not received the same level of attention compared with monitoring of the other vital signs such as blood pressure and heart rate [CBH08]. McBride et al. showed the lack of consideration towards respiratory rate reporting that only 30% of patients have their respiratory rate recorded daily [MKP05]. Reasons include the lack of a reliable and unobtrusive respiration rate measurement systems [CCH07a]. Hospitals pay less attention to respiratory rates due to the fact that current monitoring systems require direct contact with the skin [KM67]. Other methods such as video analysis to infer breath rate are non-contact, however, there are issues with privacy and low light level at night. Thus, in many hospitals, medical personnel manually

measure breathing rates.

This paper introduces BreathSens, a system that unobtrusively monitors on-bed respiration. By targetting the torso region of the body, this system converts the pressure distribution to a respiratory signal. We also show a method of visualization of the breathing patterns and consistency of results for different bed tilting commonly seen in hospital environments.

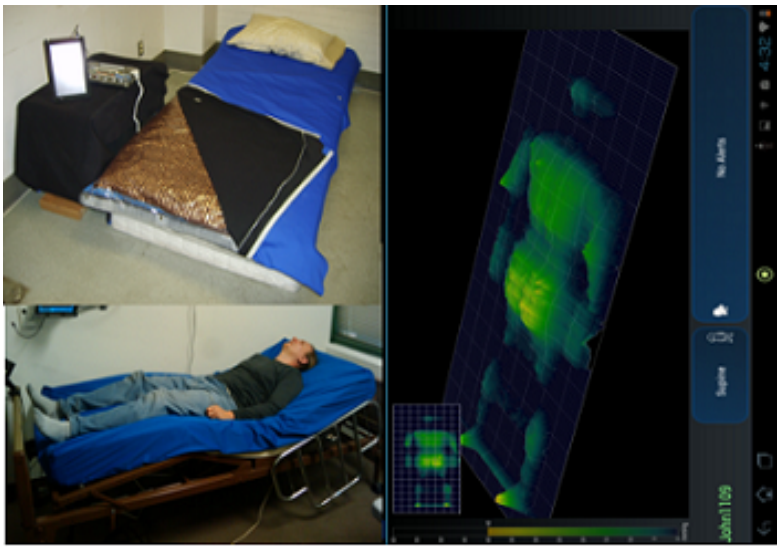

Figure 2.1: The high density pressure sensor array captures a full pressure distribution. The pressure is represented as pixel intensities.

2.2 Related Work

This section describes the current state of the art in measuring respiration rate. There are three main categories of respiratory rate monitoring: on-body, indirect contact, and non-contact.

On-body sensors are either directly attached on the skin or wearable through straps. The main problem with on-body sensors is their obtrusive nature and setup issues. Hospitals use pulse oximeters, such as the Nellcor Respiratory Monitor [Cov], to estimate respiratory rate from oximetry measurements on the pa-

tient's finger. However, the results are often inaccurate when patients have abnormal levels of oxygen saturation or low pulses [DeM07]. Respiratory Inductance Plesthysmography (RIP) is a dual belted sensor worn around the chest and abdomen. As patient's body expands and contracts during breathing, this sensor reflects changes in the inductance of its coils [KM67]. Now, many sleep centers use this sensor solution, which is recommended by the American Academy of Sleep Medicine [Car08].

The second category of respiratory rate monitoring is indirect contact. This method typically involves sensors embedded in the mattress, sheet or pillow, which overcomes the discomfort issues inherent with on-body sensors. An air mattress sensor system [CHY05] allows measurement of the respiration and heart beat movements without use of any on-body sensor. However, the shape, type, or thickness of the mattress may introduce noise to the sensed data. Another type of indirect contact sensor is capacitance sensor which measures the changes in electrical permittivity above the sensor caused by air in the lungs [HTW10]. Again, it required the subject to be localized directly above the sensor. Using hetero-core fiber optic pressure sensors, Nishyama et al. [NMW11] relaxed the restriction of sleep pose a little further by having a wider sensitivity to small pressure changes and could account for large changes.

The third category of respiratory rate monitoring is non-contact. For instance, using video or other electromagnetic radiation sensing [XGL12]. Current development in video analysis can measure respiratory rate and heart rate by analyzing the small changes in color of subjects' faces [PMP10]. The Philips Vital Signs Camera [Phi] application on iOS devices performs this contact-less measurement of breathing rate. However, using video cameras leads to a concern about patient privacy in hospital, and lighting during the night can be a significant problem. The use of infrared sensors can diminish some of these issues. Murthy et al. used an infrared imaging system to detect the temperature change of exhaled air out

of patients' mouths [MPT04].

In summary, non-contact based respiratory rate monitoring has the advantage in non-invasiveness, however still suffers in accuracy and reliability. Contact sensors need to be localized to the appropriate area. On the other hand, our system, a high density pressure sensitive bed sheet, is non-invasive, comfortable and can measure respiration at any location on the mattress.

2.3 Pressure Sensitive Bedsheet System

The designed prototype bed sheet is a 2.5m $\times$ 1.25m system that contains 64 $\times$ 128 pressure sensors (see Figure 2.1). 64 column conductive lines and 128 row conductive lines generate 8192 intersections. A sheet of e-Textile fabric which is regular fabric coated with piezo-electric polymer is located in between the row and column layers. Therefore, each joint intersection forms a pressure sensor within the three-layer sandwich structure (the resistance of the e-Textile changes when pressure is applied [RXS10]). Because of the fabric, the feel of the sensing system is just like regular fabric.

A sampling unit is connected to all conductive lines and performs matrix scanning to measure pressure map sequences. Retrieved pressure map signals of the 8192 sensors are quantified to values ranging from 0 to 255 [XLH11, LXH13]. Sampling rate is adjustable up to 10Hz. For this respiratory rate measurement, a sampling rate of 1.5Hz was used . This allows the system to achieve a maximum breathing detection rate up to 45 breaths per minute according to the Nyquist rule.

2.4 Breath Monitoring Algorithm

The method for monitoring respiration rate is composed of three parts: torso localization, respiratory signal extraction, and peak detection (see Figure 2.2). Locating the torso area in the time-indexed pressure images reduces interference caused by extremities movement. The torso localization algorithm is based on a pictorial model and cost minimization method. Mismatch and deformation costs combine as the overall cost to most accurately fit a pictorial model into a pressure image. The algorithm aims to find the best-fit among all possible configurations in the pressure image. Once the torso area is localized, the pressure values in the area of chest and stomach are used to extract respiratory signals using a vertical weighting calculation. A peak detection algorithm with adaptive thresholding is applied to mark breathing events and intervals. Figure 2.2 shows the overview of the algorithm.

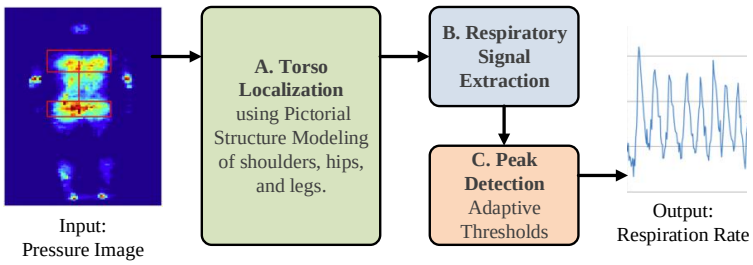

Figure 2.2: Respiration monitoring flow consists of three components: A. torso localization; B. respiratory signal extraction; C. peak detection.

2.4.1 Pictorial Model-based Localization

The torso localization method is based on the pictorial structures model proposed by Fischler and Elschlager [FE73] for identifying structured objects in images. Felzenszwalb and Huttenlocher improved the matching efficiency of the parts based algorithm using distance transforms within dynamic programming [FH03].

A simplification of the model is presented here and we apply it to finding the bodyparts in pressure images.

A graph model can be used to represent the human body. Each part of the human body can be represented as a node in a graph, e.g. shoulders, hips, upper legs, and lower legs are nodes connected by edges. In this method, the appearance of a bodypart j is measured using a mismatch cost $m_j(I, l_j)$ where I is the image and $l_j = (x_j, y_j, \theta_j)$ is the center location and rotation of the bodypart. A low value of mismatch means the bodypart model is well recognized at that location and rotation. The calculation for mismatch cost is described in Section 2.4.1.1.

In addition to this appearance cost for each bodypart model, there is a cost which measures the relationship between bodypart locations, called the deformation cost $d_{ij}(l_i, l_j)$. For bodyparts i and j, it gives a measure of the error of their expected separation. For instance, the hip and shoulders are known to be separated by the spine length. The calculation for deformation cost is described in Section 2.4.1.2.

So for a given set of bodypart models and relationships between them, the best configuration of bodyparts $L = (l_1, ..., l_n)$ in an image minimizes the total cost of mismatch for all parts and deformation between all pairs of parts:

$$\arg\min_{L} \left(\sum_{allparts} m_j(I, l_j) + \sum_{allpairs} d_{ij}(l_i, l_j) \right). \tag{2.1}$$

For n bodyparts, the calculation of this expression grows exponentially. However, with the tree representation of bodyparts, it can be solved more efficiently as a chain of computations using dynamic programming. For any leaf node (having no children), its best location $\hat{l}_j$ can be calculated as a function of its parent location l_i. So the best leaf node location is a function of parent location:

$$B_j(l_i) = \arg\min_{l_j} \left(m_j(I, l_j) + d_{ij}(l_i, l_j) \right). \tag{2.2}$$

For a non-leaf, non-root node, its best location $\hat{l}_j$ as a function of its parent location l_i is given by

$$B_j(l_i) = \arg\min_{l_j} \left(m_j(I, l_j) + d_{ij}(l_i, l_j) + \sum_{Ch(j)} B_c(l_j) \right), \tag{2.3}$$

where $Ch(j)$ means children of j, and $B_c(l_j)$ are the costs of the best locations of the children of j. This is already calculated and memorized via the dynamic programming methodology.

Then for the root node (no parent), its best location is

$$\hat{l}_j = \arg\min_{l_j} \left(m_j(I, l_j) + \sum_{Ch(j)} B_c(l_j) \right), \tag{2.4}$$

where $B_c(l_j)$ is known for each of the children of j. This formulation, Equations (2.2) to (2.4), reduces the number of computations from exponential to polynomial while still producing the globally best solution.

2.4.1.1 Compute Mismatch Cost

To compute the mismatch cost $m_j(I, l_j)$ for each bodypart, we select a representative template. The bodyparts are simply represented as rectangular boxes surrounded by a border (see Figure 2.3 which shows an example of the shoulder and hip models). To account for different pressure images with varying weights of subjects, the image I is binarized at different thresholds. A convolution operation of this kernel with the binary images efficiently gives the mismatch cost at all locations. This computes how many pixels do not match inside the inner box and within the border. Then, the mismatch cost is the smallest cost across all threshold levels for each location.

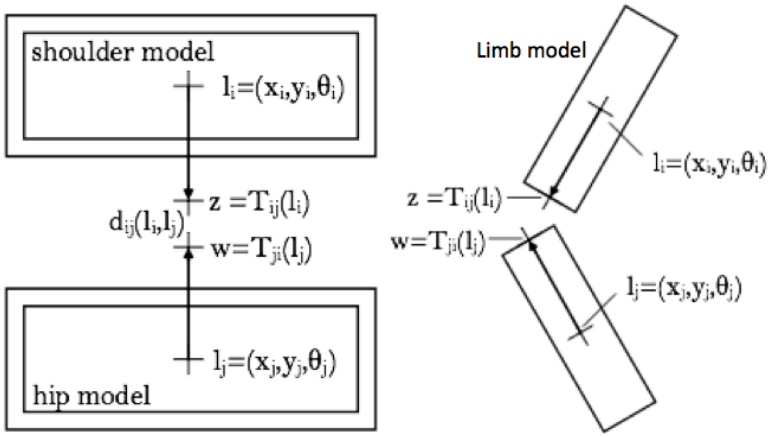

Figure 2.3: Transformation of bodypart models. The locations of the bodypart models are transformed into a common space which allows the calculation of a deformation cost.

2.4.1.2 Compute Deformation Cost

To compute the deformation cost $d_{ij}(l_i, l_j)$ between bodyparts, we define this cost to have the form

$$d_{ij}(l_i, l_j) = ||T_{ij}(l_i) - T_{ji}(l_j)||. \tag{2.5}$$

This is a simple distance metric between locations transformed to a common space (refer to Figure 2.3). The transforms can be translations, rotations, and scaling, hence they are invertible. The effect of the transforms is to specify the expected relations between the locations. I.e. if two bodyparts have no deformation cost and are correctly positioned, then the transformed locations will coincide. The pairwise distance metric takes quadratic time in the number of locations. For every location of the parent, we want to compute the distance to each location of the child. On the surface, quadratic time may seem satisfactory but this can be improved to linear time through the use of distance transforms [Bor86]. In fact, every pairwise distance between l_i and l_j need not be computed. From Equation (2.2), only the smallest sum of deformation cost and mismatch cost is

needed at each location of l_i. Sample pseudo code is shown in the Algorithm 1.

Algorithm 1: Pictorial Model Localization

Input: mismatch cost, m; deformation cost, d; image, I;

center and rotation of the bodypart, $l = (x, y, \theta)$

Output: best configuration of bodyparts, $\hat{L}$

Initialize: $\hat{L} = 0$, $B = 0$,

1: **for** all leaf location l_j in bodyparts **do**

2: $l_i = l_j$'s parent location

3: $B_j(l_i) = \arg\min_{l_j} (m_j(I, l_j) + d_{ij}(l_i, l_j))$

4: $\hat{L}(l_j) = B_j(l_i)$

5: **end for**

6: **for** all internal node location l_j in bodyparts **do**

7: $l_i = l_j$'s parent location

8: $B_j(l_i) = \arg\min_{l_j} (m_j(I, l_j) + d_{ij}(l_i, l_j) + \sum_{Ch(j)} B_c(l_j))$

9: $\hat{L}(l_j) = B_j(l_i)$

10: **end for**

11: **for** root location l_j in bodyparts **do**

12: $\hat{l_j} = \arg\min_{l_j} (m_j(I, l_j) + \sum_{Ch(j)} B_c(l_j))$

13: $\hat{L}(l_j) = l_j$

14: **end for**

15: Return $\hat{L}$ as best configuration of bodyparts

2.4.2 Respiratory Signal Extraction

This subsection describes the respiratory signal extraction method from the time series pressure regions. This results in a pressure indicator which is based on an observation that, while breathing, the pressure distribution along with vertical direction (from chest to stomach direction) varies with certain patterns and

rhythms. For every frame, the pressure indicator sums the pressure values with their corresponding vertical directional coordinates:

$$Resp(t) = \sum_{(x,y)\in torso} \sum y * I[x, y](t). \tag{2.6}$$

The range of the pixels in the torso is the region between chest and hip bounding boxes which is enclosed by the bottom of the shoulder bounding box and the top of the hip bounding box. The calculated pressure indictor forms a time-series respiratory signal stream.

2.4.3 Peak Detection with Adaptive Thresholding

In general, a simple peak detection algorithm [Bil] is sufficient to recognize the periodic peak and valley of the time series data. However, arbitrary thresholding does not always work since the magnitude difference between peak and valley of time series data varies among testing subjects. Subjects breathing with moderate muscle activity in their shoulder or back area tend to generate large magnitude differences in the calculated pressure indictor time series. To accommodate the differences among subjects, the selected peak detection algorithm is augmented with adaptive threshold version as shown in the Algorithm 2.

Given a time series data of the extracted respiration signal, this adaptive threshold method profiles the relationship between the number of breaths and threshold values. A threshold is defined as the value difference by which a peak is recognized from surrounding data. So for each threshold value between 0 and the maximum magnitude difference in the data, the algorithm detects a peak when the data falls below the peak value by more than the threshold value. Similarly, a valley is detected when the data rises above the valley value by more than the threshold. Once all thresholds have been tested, it then finds the range of thresholds that have the least effect on the number of breathing events. This coincides with the flat area (see Figure 2.4). It means that, within certain threshold

Algorithm 2: Peak Detection with Adaptive Thresholds

Input: time series $data$ of size n

Output: number of detected breaths

Initialize: $lookformax$=true

1: $maxdiff$ = maximum magnitude difference in $data$
2: **for** $thresh = 0$ to $maxdiff$ **do**
3: **for** all n points in $data$ **do**
4: **if** $lookformax = true$ and $data.value < currentmax - thresh$ **then**
5: Peak detected and set $lookformax$ = false
6: **else**
7: Update $currentmax$
8: **end if**
9: **if** $lookformax = false$ and $data.value > currentmin + thresh$ **then**
10: Valley detected and set $lookformax$ = true
11: **else**
12: Update $currentmin$
13: **end if**
14: **end for**
15: Record the number of breaths (peak and valley pairs) and the corresponding $thresh$ in graph
16: **end for**
17: Find the first flat region in graph and output the number of detected breaths

ranges, the number of breathing events is consistent and implies those thresholds are less sensitive to the random hardware noise. The number of breathing events is recorded and the corresponding event intervals are used to calculate respiratory rate. A period of peak and valley is viewed as a complete respiration and the intervals between two peaks are viewed as breath intervals.

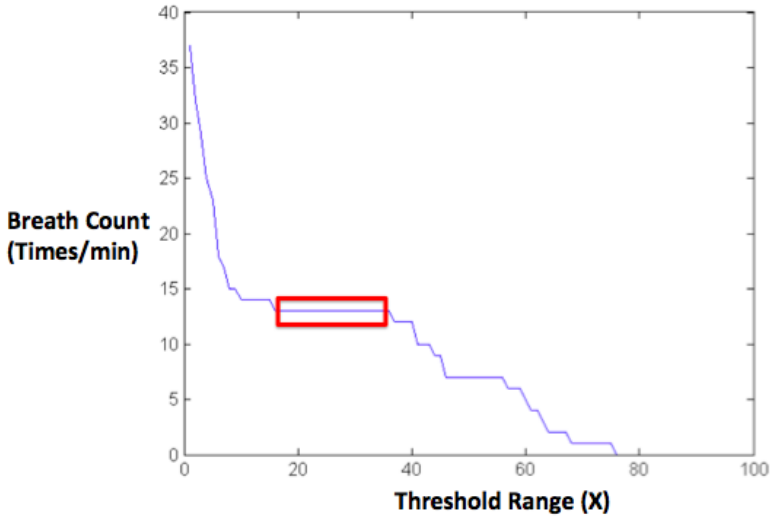

Figure 2.4: Number of detected breaths for threshold values

2.5 Evaluation

Table 2.1: Information of the 12 participants

ID	Gender	Height(inch)	Weight(lb)	BMI
1	M	67	173	27.09
2	M	75	165	20.62
3	M	73	182	24.01
4	M	66	176	28.40
5	F	63	102	18.07
6	M	65	160	26.62
7	F	65	108	17.97
8	M	70	140	20.09
9	M	72	167	22.65
10	M	69	143	21.12
11	M	68	150	22.80
12	M	70	178	25.54

12 subjects participated in the study with heights 63 to 75 inches, weights 102 to 182 pounds. Their gender, height, and weight information were recorded in Table 2.1 and used in human model construction. The high density pressure sensor sheet was deployed on top of a foam mattress with memory in a lab environment. The experimental goals were to evaluate the effectiveness of the torso localization algorithm for respiratory signals extraction on a regular soft bed environment. During experiments, subjects were allowed to lie in their preferred posture and keep their regular lying habits. In addition, data was recorded in full without segmentation and truncation due to interferences caused by extremity movements. Full experiment processes were taped, breath events were timed and labelled manually from the taped videos according to the visible chest wall movement. Recording started when the subjects lied on top of the pressure sensing system in their preferred lying posture. They were asked to breathe as usual and not to make any large posture changes, such as rolling or sliding, during the recording. Furthermore, tilted bed situations as commonly seen in clinics were simulated by changing the tilted angles of the bed head and foot areas. For these tilted bed situations, the subjects were evaluated in supine posture only.

2.5.1 Results of Model-based Localization

Table 2.2 summarizes the accuracy of bodypart localization for the 3 postures compared against prior work by Farshbaf et al. [FYP13] and Grimm et al. [GSH11]. We use the same metrics as described in the prior work, where error is measured by Euclidean distance in inches between the tested and ground truth locations, and accuracy is calculated as the percentage of bodyparts that have error of less than 1 inch. In these experiments, the elbow resulted in the lowest localization accuracy. This can be explained by the relative weakness in pressure compared to the high pressure of the shoulder.

Table 2.2: Accuracy of bodyparts localization

Posture	Bodypart	Accuracy(%) Farshbaf	Error(inch) Grimm	Accuracy(%)	Error(inch)
Supine	Shoulder	93.3	1.7	92.4	1.2
	Left Elbow	86.7	-	87.1	1.6
	Right Elbow	80.0	-	86.2	1.7
	Sacrum	93.3	1.7	94.7	0.9
	Left Heel	80.0	-	93.1	1.0
	Right Heel	80.0	-	93.7	1.0
Left	Shoulder	86.7	2.9	94.5	0.9
	Elbow	76.7	-	82.1	2.2
	Hip	93.3	2.0	91.9	1.3
	Knee	-	3.3	90.0	1.8
Right	Shoulder	90.0	2.3	92.1	1.2
	Elbow	96.7	-	84.5	2.0
	Hip	90.0	2.0	92.2	1.2
	Knee	-	3.3	85.2	2.0
Average		85.7	2.7	89.8	1.4

2.5.2 Results of Respiration Monitoring

Table 2.3: Respiration results in three common lying postures (detected breaths/ground truth)

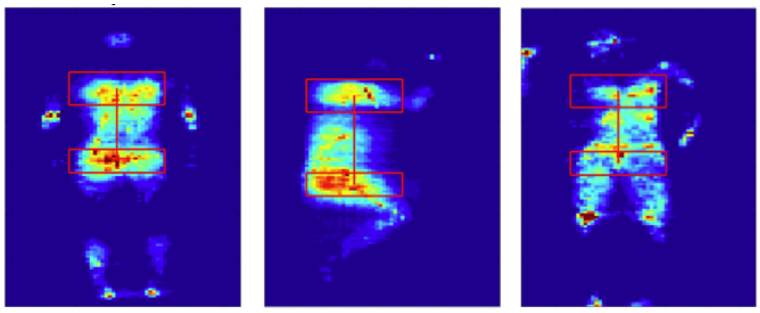

ID	Supine	Lateral	Prone
1	174/176	169/172	176/177
2	147/155	137/154	143/152
3	171/175	162/173	170/175
4	184/185	184/186	187/188
5	127/130	125/133	130/127
6	136/142	138/144	139/144
7	155/162	162/162	157/160
8	179/177	174/176	172/175
9	160/166	158/167	162/166
10	138/144	137/142	139/141
11	164/168	170/172	168/172
12	152/150	147/146	148/148
Avg.	**157.5/160.8**	**155.3/160.6**	**157.6/160.4**
Error	**2.0%**	**3.3%**	**1.8%**

Pressure values variation within the torso region is of most interest for respiratory signal extraction. In this experiment, respiratory signals were extracted

from pressure image sequences when participants lied in common lying postures: supine, side, and prone for 10 minutes each. The method of torso localization was applied to the pressure image sequences to keep track of the regions between chest and stomach areas. Then signal extraction via vertical weighting calculation and peak detection methods were used to extract breathing events. Table 2.3 summarizes the results and shows comparisons between the detected respiration events and the ground truth visually recognized from video recordings for all three lying postures. On average, the detected respiration events match well with ground truth across the three common lying postures. Different lying postures and extremities movements did not affect the quality of torso localization and the extracted respiratory signals.

2.5.3 Visualization of Respiration Motion

It is useful to illustrate the effect that vertical weighting calculation makes on respiratory signal extraction. There is an apparent geometrical delay from chest to stomach area and weighted pressure values with its vertical coordinates relative to the bounding box border emphasizes the respiration pattern. Visualizing the vertical momentum calculation can be a useful tool to investigate the nature of the geometrical delay phenomenon in pressure image sequences.

In order to visualize calculated vertical momentum, results from peak detection algorithm are used. Peak detection algorithm returns a series of peaks and valleys from the pressure indicator time series. By subtracting two consecutive peak and valley indexed pressure images, the differences between images of peaks and valleys are obtained. Figure 2.5 visualizes the peaks and valleys of respiration by averaging the pressure differences between peaks and valleys. To better visualize the difference of chest and stomach area, all positive differences were marked as black and negative differences were marked as white. Gray area stands for no obvious pressure differences. It can be seen that pressure distribution of chest

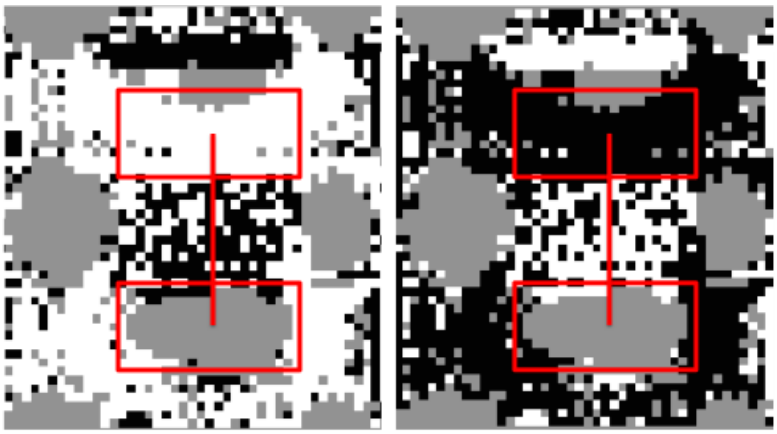

Figure 2.5: Examples of change in pressure distribution for inhaling and exhaling events. The red boxes show the location of detected shoulder and hip regions. The black and white areas show the locations of the greatest pressure change.

area is in opposite phase of the stomach area. This opposite phase phenomenon explains the reason why vertical weighting calculations can be a useful indicator for respiratory patterns extraction, because the geometrical delay from chest to stomach region is included in the indicator calculation.

2.5.4 Comparison of Body Region Locations

Three scenarios were evaluated and compared to demonstrate the importance of torso tracking: signals from the whole sheet without applying torso localization algorithm, signals from half of the sheet and centralized in the center of the weight, and signals from torso localized area, same as the results presented previously. The difference between the estimated breathing events and ground truth are reported in Table 2.4 for the supine posture.

Extracted respiratory events from torso localized areas showed good consistency with the ground truth. This is because during breathing, large periodic pressure variances are expected in the chest to stomach regions. Pressure variance outsides the torso regions can be viewed as interference which directly impacts the calcula-

tion of vertical weighted signal extraction. Interference caused by the extremities movements were time-varied and subject-dependent; therefore, the accuracy of respiratory signal extraction from the whole sheet largely was highly impacted by the movements of the participants. For the case of extracting signals from the area nearby the center of mass, the accuracy of respiratory signal extraction was reduced because the targeted area included parts of extremities. In summary, respiratory signal extraction with torso localization effectively reduces the interference caused by the extremities movement, and the accuracy of respiratory signals were less varied across subjects.

2.5.5 Respiration in Tilted Bed Environment

Another common scenario of sleep environment in clinics is tilted bed setup. Tilted bed environments change the original pressure distribution underneath a human body. Hence, it is necessary to evaluate the effect of tilted environment on respiratory signal extraction. Figure 2.6 shows pressure image samples from tilted environment with raised head (15°), raise knee (15°), and both raised head and knee. Although pressure distribution changed with degree of tilting, the areas of chest and stomach were still visually recognizable. Pressure redistribution caused by tilted bed environment has limited effect on body contact area size and the pressure values in chest and hips areas are still prominent compared to other regions. However, the main difference is the distribution of pressure within the body profile.

In this experiment, participants were requested to lie in supine position for 5 minutes of recording. Results of Figure 2.7 reveal that respiratory signals can be extracted from tilted bed environment and show consistency. Actually, it is worth noticing that much under body pressure was accumulated in the chest area for the case of raised knee tilting; hence, the interference caused by the upper extremities movements had larger weight in the vertical weighting calculation. On the other

Table 2.4: Comparison of the standard deviation between the estimated breathing events and the ground truth within full sheet area, by the center of mass, and by torso localization

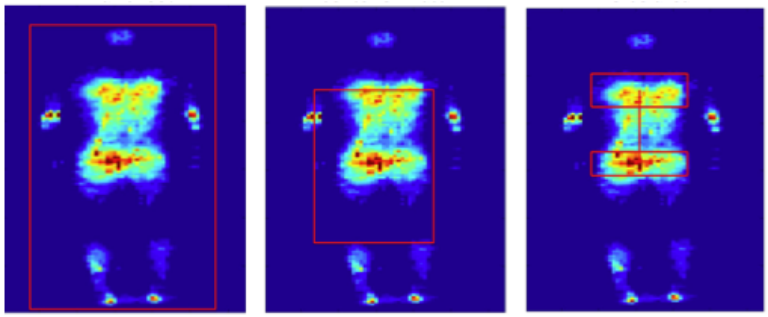

ID	**F**ullsheet	**C**enter of Mass	**T**orso Area
1	11	10	2
2	14	9	4
3	-8	-6	-3
4	-8	-4	-1
5	12	8	3
6	-7	-2	-2
7	6	1	3
8	-6	-5	-3
9	11	9	4
10	8	8	2
11	4	5	3
12	-9	-7	-2
Ave.	**9.18**	**6.67**	**2.79**
Error	**5.7%**	**4.1%**	**1.7%**

hand, much under body pressure was accumulated in the stomach and hip area for the case of the raised head tilting; hence, the interference caused by the lower extremities movements had larger impact on the respiratory signals extraction.

Therefore, torso localization becomes more important in a tilted bed environment because redistributed pressure tends to increase the weight of extremity movements. Slight extremities movement may incur large interference to respiratory signal extraction.

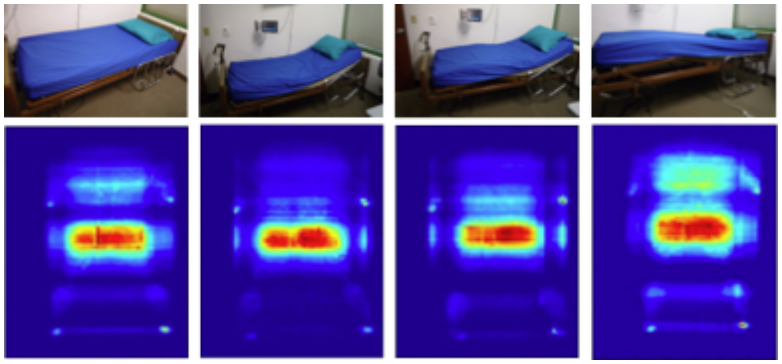

(a) Original (b) HeadLift (c) EndLift (d) BothLift

Figure 2.6: Tilted bed setup

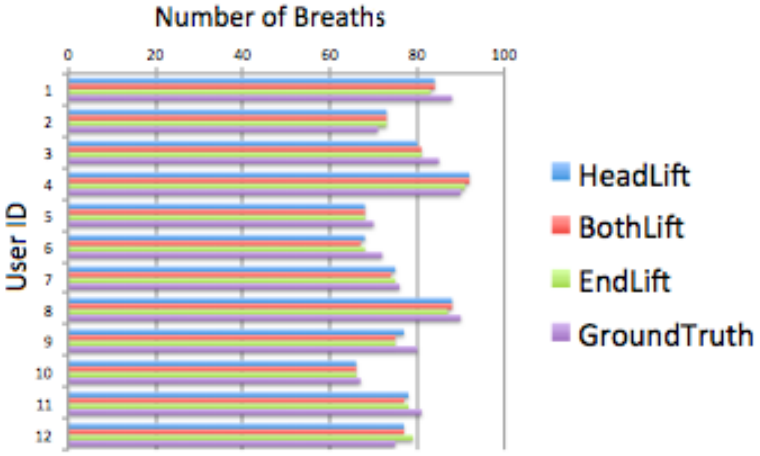

Figure 2.7: Breath count comparison for each subject on a tilted bed

2.6 Conclusion

The ability to continuously monitor respiration rates of patients in homecare or in clinics is an important goal. Past research showed that monitoring patient breath-

Table 2.5: Respiration monitoring in different tilted bed environment

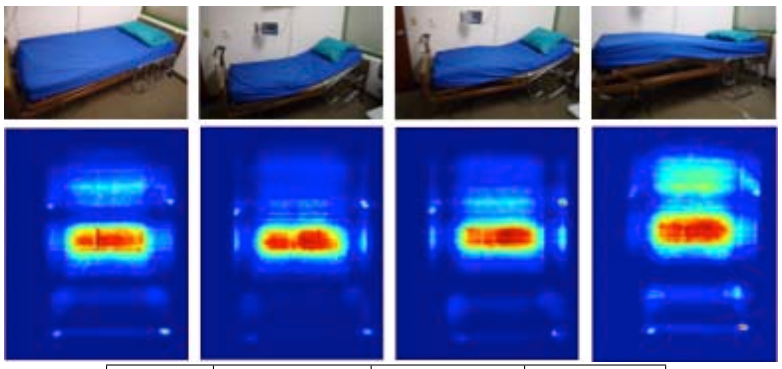

ID	**H**eadLift	**B**othLift	**E**ndLift
1	84	84	83
2	73	73	73
3	80	81	81
4	92	92	91
5	68	68	68
6	68	67	68
7	75	73	75
8	88	88	87
9	77	75	75
10	66	66	66
11	78	77	78
12	77	77	79
Avg.	**77.17**	**76.75**	**77.0**

ing can lower the associated mortality rates for long-term bedridden patients. Nowadays, in-bed sensors consisting of pressure sensitive arrays are unobtrusive and are suitable for deployment in a wide range of settings. Such systems aim to extract respiratory signals from time-series pressure sequences. However, variance of movements, such as unpredictable extremities activities, affect the quality of

the extracted respiratory signals. BreathSens, a high density pressure sensing system made of e-Textile, profiles the underbody pressure distribution and localizes torso area based on the high resolution pressure images. Pictorial Structure models is introduced to localize pressure distribution of the body. With the robust bodyparts localization algorithm, respiratory signals extracted from the localized torso area are insensitive to arbitrary extremities movements. A pilot study including 12 subjects reveals that the proposed method enables reliable localization of body parts and demonstrates BreathSens's capability of respiratory monitoring with variations of sleep postures, locations, and commonly tilted clinical bed conditions.

CHAPTER 3

Contactless Vital Signs Monitoring

3.1 Introduction

Among the various medical signals, vital signs (i.e., heart rate and respiratory rate) are the most crucial measures used to assess bodily functions and monitor illness progression to determine the effective treatments that should be administered [DBG05]. Furthermore, vital-sign measurements are helpful in predicting potential clinical events. For example, the variation in respiratory rate is a marker for cardiac arrest or admission to an intensive care unit [CCH07b].

Several off-the-shelf home devices are used measuring vital signs [Omr, For]. They require users to follow the instrument instructions strictly and to perform the measurements under controlled conditions. For example, when a person uses an electrocardiography (ECG) device to measure heartbeat, the electrode should be attached on the correct parts of the body and the person should not talk while conducting the measurements. Therefore, consistently obtaining valid vital sign measurements without the assistance of medical personnel is difficult. Moreover, because using these devices is inconvenient, patients are unlikely to perform vital sign measurements by themselves.

For years, the research community has investigated unobtrusive methods for vital sign measurement. Generally, existing work can be classified into three categories. The first category is based on direct skin contact. During measurements, a device must be in direct physical contact with the body of the user. Valchinov et

al. developed a dry skin electrode that reduced contact impedance and variation and motion artifacts [VP04].

The second category is based on indirect contact (i.e., sensors that do not require direct physical skin contact). Under-bed mattress sensors have been used to measure heartbeat, respiration, and body movements using thin, air-sealed [WWT05], film [Bed], or hydraulic [HS10] pressure sensors. Chi et al. [C-NK10] developed a capacitive electrode to measure heart rate that can function through clothing.

The third category is based on noncontact techniques. Noncontact techniques enable monitoring vital signs remotely and seem appealing for users. Aoki et al. [ATM01] discussed a nonrestrictive visual sensing method for detecting respiration patterns by using a fiber grating camera and processor unit. Zhu et al. [ZFP05] developed an infrared-camera-based system to monitor respiration and infer the associated heart rate. Chekmenev et al. [CRF05] used a thermal camera consisting of a focal plane array for a long-wave infrared sensor to extract heart rate and respiration from temperature changes. However, all of the aforementioned noncontact methods involve using sensors that are sensitive to changes in environmental factors such as light or temperature, and no robust calibration methods for compensating for these changes have been developed.

In this paper, a low-cost microwave Doppler-radar-based system complementary to existing noncontact techniques is presented. According to Doppler theory [Bla96], signals reflected by objects exhibit a quantitative phase change, called Doppler shift, because of the movement of the objects. The magnitude of the phase change is sufficiently large for measuring heartbeat and chest wall movement. A novel framework based on the Doppler radar structure and signal model was proposed to automatically demodulate the Doppler radar signals and extract the heart and respiratory rates without precalibration.

3.2 Doppler Radar Preliminaries

The Doppler effect was proposed by Christian Doppler in 1842 and has since been widely applied in motion detection. Microwave Doppler radar was first applied to measure respiratory rate and detect sleep apnea in 1975 [Lin92]. A Doppler radar transmits a continuous-wave signal, which is reflected by a target and then received and demodulated by a receiver. According to Doppler theory, the position-varying information is proportionally demodulated in the reflected signal when the net velocity is zero. Therefore, the chest wall movement caused by volume change during respiration can be detected using the Doppler-radar motion-sensing system. Because of the advances in wireless transmission and electronic devices, using in-phase and quadrature (I/Q) Doppler radar for heartbeat detection is feasible [DLL04, CLL08].

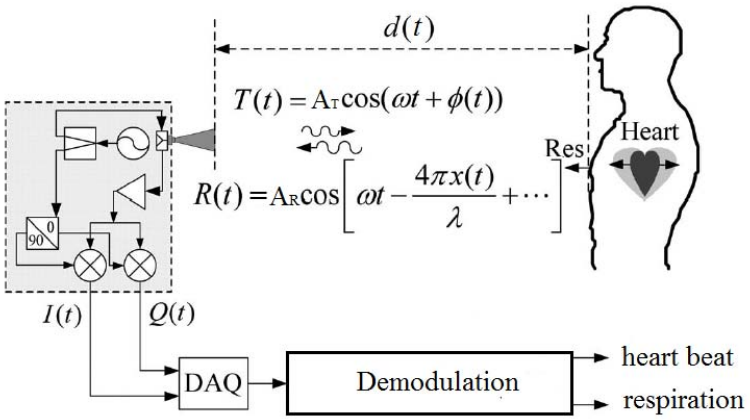

Figure 3.1: The I/Q Doppler radar block diagram for non-contact vital sign monitoring

3.2.1 In-phase/Quadrature I/Q Doppler Radar

Figure 3.1 shows the operation theory and block diagram of an I/Q Doppler radar for non-contact vital sign measurement. The Doppler radar system transmits the continuous-wave signal $T(t)$:

$$T(t) = A_T \cos(\omega t + \phi(t)), \tag{3.1}$$

where A_T is the amplitude of the carrier signal, $\omega = 2\pi f$ denotes the angular velocity (carrier frequency), and $\phi(t)$ represents the time-varying phase information of the transmitted signal.

The subject is at a distance d_0 from the radar and the total traversal distance of microwave signal is $d(t) = 2(d_0 + x(t))$, where $x(t)$ is the time-varying displacement caused by heart beat and respiration.

The transmission wave is reflected by the subject and received at Doppler radar as $R(t)$:

$$R(t) = A_R \cos[\omega t - \frac{4\pi d_0}{\lambda} - \frac{4\pi x(t)}{\lambda} + \phi(t - \frac{2d_0}{c})], \tag{3.2}$$

where A_R is the amplitude of the received signal, $\lambda = c/f$ is the wavelength of the carrier signal, and c is the speed of light. We can see that the time-varying displacement $x(t)$ is modulated in the phase change of the received signal. As shown in Figure 3.1, $R(t)$ is down-converted by $T(t)$ and then generates two baseband signals. One is the in-phase signal, denoted by $I(t)$:

$$I(t) = A_I \cos[\frac{4\pi x(t)}{\lambda} + \frac{4\pi d_0}{\lambda} + \phi(t - \frac{2d_0}{c})] + DC_I, \tag{3.3}$$

and the other is the quadrature signal, denoted by $Q(t)$:

$$Q(t) = A_Q \sin[\frac{4\pi x(t)}{\lambda} + \frac{4\pi d_0}{\lambda} + \phi(t - \frac{2d_0}{c}) + \phi_0)] + DC_Q, \tag{3.4}$$

where A_I is the amplitude of in-phase signal, A_Q the amplitude of quadrature signal, and ϕ_0 is the phase offset between $I(t)$ and $Q(t)$. DC_I and DC_Q are the DC offsets in I/Q channels, respectively. The ratio between A_I and A_Q is called gain imbalance, and ϕ_0 is called phase imbalance. Both gain imbalance and phase imbalance are caused by circuit imperfection.

$I(t)$ and $Q(t)$ are then digitized by the data acquisition block (DAQ), and the phase change, $x(t)$, is demodulated for heart beat and respiration measurement. For the simplicity of presentation, we neglect the constant phase offset, $4\pi d_0/\lambda + \phi(t - 2d_0/c)$, in the I/Q receiver and use the following equations to describe the baseband signals:

$$I(t) = A_I \cos(\frac{4\pi x(t)}{\lambda}) + DC_I, \tag{3.5}$$

$$Q(t) = A_Q \sin(\frac{4\pi x(t)}{\lambda} + \phi_0) + DC_Q. \tag{3.6}$$

3.2.2 The Challenge

As shown in Figure 3.1, the demodulation module processes the baseband signals, $I(t)$ and $Q(t)$, for heartbeat and respiration information extraction. If the circuit in the Doppler radar is perfect, then no gain or phase imbalance occurs (i.e., A_I in Eq. (3.5) is equal to A_Q in Eq. (3.6), and ϕ_0 in Eq. (3.6) is equal to zero).

Based on these ideal-case assumptions, several techniques have been proposed in the extant literature for demodulating Doppler radar signals to extract vital signs. Droitcour et al. approximated I/Q signals as linear formulas when the responding phase was small, and then extracted vital signs by using the tuning carrier frequency [DLL04]. Tao et al. converted transmission waves to a set of pulse signals and detected the phase change according to its peaks [TLW09], whereas Lee et al. proposed a reassigned joint time-frequency transform to track the heart rate [LYK11].

Lubecke et al. presented various demodulation methods involving the precalibration of dc offsets [PLL07, MLM09, BLP09]. Li and Lin formulated I/Q signals into a complex vector to perform Fourier analysis, and the phase change was calculated using iterative spectrum comparison [LL08].

These existing demodulation methods have two main drawbacks. First, these methods require either approximating I/Q signals [DLL04, TLW09] or accurately precalibrating the dc offsets [LL08, PLL07]. Both the electronic components and multichannel transmission and reflection, which is related to the environment, produce dc offset. Therefore, the dc offsets in the I/Q channels must be recalibrated whenever the environment changes, which is not applicable in practice. Fletcher and Han used dual beams to target various locations; one location was used as a reference [FH09]. Second, these methods involve the assumption that circuit components are perfect in that the gain and phase imbalances are minimal. In real radar systems, the effect of gain and phase imbalance is considerable. Park et al. [PYL07] measured the imbalance factors in a direct-conversion quadrature radar circuit and reported that imbalance is unavoidable. In their experiments, the gain imbalance was 4.7 and the average phase imbalance was 18.5 degrees. Thus, phase imbalance has a severe negative effect on error the rate in signal demodulation [ZH05]. Therefore, developing an accurate and robust signal-processing technique for signal demodulation in Doppler radar systems is necessary. In the application used in this study, the associated challenges are:

1. Accuracy: the demodulation method should account for all parameters (i.e., A_I, A_Q, ϕ_0, DC_I, and DC_Q) in the signal model and directly extract the motion component $x(t)$ accurately from the I/Q signals;

2. Self-calibration: the environment might change, causing the signal model to change during measurement. The demodulation method can self-calibrate and tolerate the parameter changes. No manual setup is required.

3.3 Vital Signs Monitoring System

In this section, the proposed Doppler radar system for noncontact self-calibrating vital-sign measurement is introduced. Figure 3.2 shows an overview of the struc-

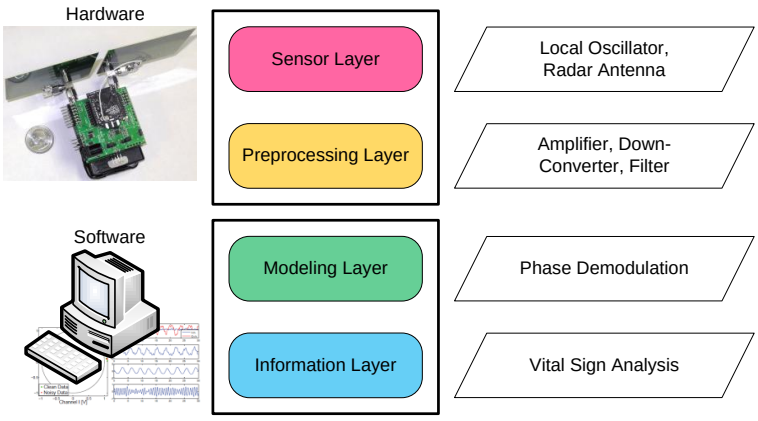

Figure 3.2: The layered structure of non-contact self-calibrating vital sign measurement system, including sensor layer, pre-processing layer, modeling layer, and information layer.

ture of this system, which comprises four layers: the sensor, preprocessing, modeling, and information layers. The sensor layer and preprocessing layer were built on the hardware, whereas the modeling layer and information layer were designed using software. Each of the layers are described in the following subsections. A hardware prototype of the radar sensor is shown in Figure 3.3 with its main functional components. After preprocessing the sensed baseband radar signal, an elliptic phase model was constructed and the model parameters were calculated based on the proposed min-ℓ_1-based fitting (self-calibration). In the information layer, these self-calibrated elliptic parameters were identified to reconstruct baseband signals, perform demodulation to identify the corresponding chest wall movement, and extract respiration and heartbeat signals using spectrum analysis. The framework of self-calibration (modeling layer) and vital-sign extraction (information layer) is shown in Figure 3.4.

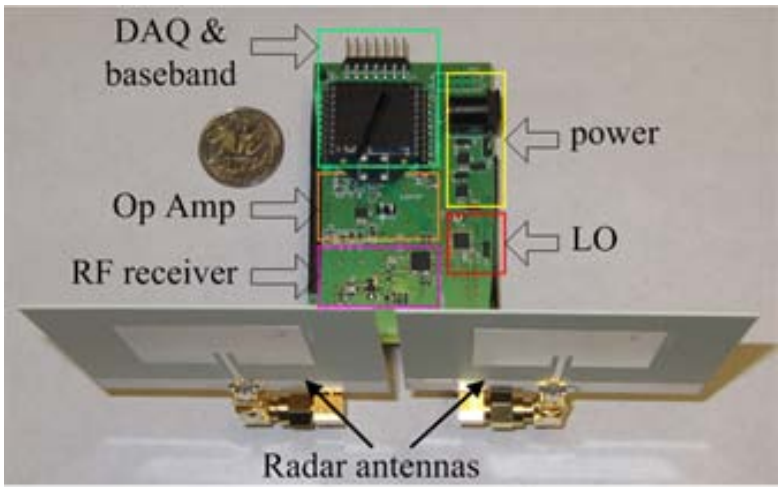

Figure 3.3: The hardware prototype of the Doppler radar vital signs measurement system.

3.3.1 Sensor Layer

The sensor layer generated a single-tone carrier signal that was transmitted to the target to gather the desired phase information [Lin92]. The key building blocks used in the sensor system are shown in Table 3.1. The radar sensor system was designed using a homodyne transceiver architecture integrated on a Rogers 4350 laminate for enhanced radio frequency (RF) performance. In this design, the sensor layer was implemented using a voltage-controlled oscillator (VCO). The single-tone signal produced by the VCO was divided by a balun into two components: one component was transmitted through a transmitter antenna to the target, and the second component served as the local oscillator (LO) signal sent to the demodulator. If the target was moving (e.g., the chest wall of the subject), then the single-tone carrier signal was modulated in the phase containing the movement information of the target, which is a process called nonlinear phase modulation [GIL, GLF12]. Although a free-running VCO was used in this design, coherent demodulation was achieved because the transmit signal and the LO signal arrived from the same signal source. The phase noise of the VCO does not

affect sensitivity in noncontact vital-signal measurements, because of the range correlation effect [DBL04]. Two patch antennas were specifically designed for use in this radar sensor system. The total transmission power was −10dBm (0.1mW).

Table 3.1: Building blocks of the radar-sensing system

Blocks	Manufacturer	Specification
VCO	Hittite	2.25-2.5GHz; Pout: 4.5dBm
Demodulator	Skyworks	RF/LO: 0.4 3GHz; Gain: 1.2dB
LNA	Hittite	2.3-2.5GHz; NF: 1.7dB; Gain: 19dB; P_{1dB}out: 6dBm
Gain Block	RFMD	Gain: 12dB; P_{1dB}out: 11dBm
BPF	Johanson	Pass band: 2400 2500 MHz
Op Amp	Maxim IC	Bias: 3V; GBW: 3 MHz
Controller	TI	Bias: 3V; 10-bit ADC

3.3.2 Pre-processing Layer

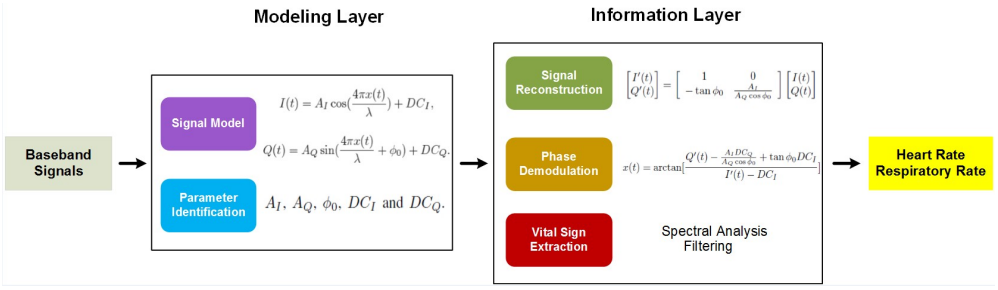

Figure 3.4: The framework of signal demodulation in a non-contact vital sign monitoring system.

The preprocessing layer was an RF receiver that received the signal from the sensor layer and down-converted it to baseband I/Q signals. A low-noise amplifier (LNA) was placed at the front end of the preprocessing layer to ensure a favorable noise figure for the receiver chain. The LNA also provided a 19-dB gain

to boost the weak signal reflected from the moving target. A ceramic band-pass filter (BPF), as shown in Table 3.1, followed the LNA to block the out-of-band interference. This is critical because an abundance of strong interference is present in the air (e.g., 900-MHz cellular signals and 5.8-GHz WiFi signals). The filtered signal was further boosted by a gain block to reach a sufficient power level for powering the RF port of the demodulator. A quadrature demodulator converted the received signal to baseband I/Q signals, which were amplified by the baseband operational amplifier (Op Amp). The Op Amp was configured with a differential input structure and the baseband gain was determined using the feedback of the amplifier. The Op Amp had a gain bandwidth product of only 3 MHz. Therefore, the Op Amp also served as a low-pass filter that preserved the low-frequency vital-sign signals and blocked any interference. The baseband output was digitized using a 10-bit analog-to-digital converter integrated in a microcontroller. After collection using an on-board data acquisition module, the digital baseband I/Q signals were transmitted to a computer for phase demodulation.

3.3.3 Modeling Layer

In the $I(t)$ and $Q(t)$ domain, samples of the I/Q signals lie on an ellipse. So the function of the modeling layer formulates the I/Q signals as an elliptic curve fitting problem and reconstruct radar signal by finding six parameters to represent the ellipse, A, B, C, D, E, G[1]. An ellipse is a special case in conic curves which can be described by:

$$F(x, y) = Ax^2 + Bxy + Cy^2 + Dx + Ey + G = 0, \tag{3.7}$$

with one constraint:

$$B^2 - 4AC < 0, \tag{3.8}$$

[1]For simplicity, we will use $A \sim G$ to represent A, B, C, D, E, G

where (x, y) are simplified representative coordinates in $I(t)$ and $Q(t)$ space.

To solve the elliptic curve fitting problem from samples of the I/Q signals, we propose ℓ_1 minimization with LMI relaxation. This will be described in the next section. The radar signal parameters (i.e. A_I, A_Q, ϕ_0, DC_I and DC_Q) that describe the transmitted and received signals are derived from the six elliptic parameters. The full derivation from elliptic formulation to radar signal parameters can be found in the submitted manuscript. After solving LMI problem and finding six elliptic parameters, the five radar signal parameters (A_I, A_Q, ϕ_0, DC_I and DC_Q) can be calculated using the equivalences below.

$$DC_I = \frac{2CD - BE}{B^2 - 4AC}, \tag{3.9}$$

$$DC_Q = \frac{2AE - BD}{B^2 - 4AC}, \tag{3.10}$$

$$A_I = \sqrt{\frac{AE^2 + CD^2 + GB^2 - BDE - ACG}{(B^2 - 4AC)[\sqrt{(A-C)^2 + B^2} - (A+C)]}} \tag{3.11}$$

$$A_Q = \sqrt{\frac{AE^2 + CD^2 + GB^2 - BDE - ACG}{(B^2 - 4AC)[-\sqrt{(A-C)^2 + B^2} - (A+C)]}} \tag{3.12}$$

$$\phi_0 = \frac{1}{2}\cot^{-1}(\frac{A-C}{B}) \tag{3.13}$$

3.3.4 Information Layer

The transmitted signal $I(t)$ and received signal $Q(t)$ models were recovered with A_I, A_Q, ϕ_0, DC_I, and DC_Q to increase the accuracy of respiration and heartbeat signal extraction. Chest wall displacement $x(t)$ was identified using the information of gain imbalance (A_I/A_Q) and phase imbalance (ϕ_0) derived from the

aforementioned signals. The Gram-Schmit procedure [Bjo67] was used to reconstruct $(I(t), Q(t))$ input.

$$\begin{bmatrix} I'(t) \\ Q'(t) \end{bmatrix} = \begin{bmatrix} 1 & 0 \\ -\tan\phi_0 & \frac{A_I}{A_Q \cos\phi_0} \end{bmatrix} \begin{bmatrix} I(t) \\ Q(t) \end{bmatrix}. \tag{3.14}$$

The reconstructed baseband signal is $(I'(t), Q'(t))$:

$$I'(t) = A_I \cos(\frac{4\pi x(t)}{\lambda}) + DC_I, \tag{3.15}$$

$$Q'(t) = A_I \sin(\frac{4\pi x(t)}{\lambda}) + \frac{A_I DC_Q}{A_Q \cos\phi_0} - \tan\phi_0 DC_I. \tag{3.16}$$

Then we can demodulate heart beat and respiration related information, $x(t)$, by the arctangent formula directly:

$$x(t) = \arctan[\frac{Q'(t) - \frac{A_I DC_Q}{A_Q \cos\phi_0} + \tan\phi_0 DC_I}{I'(t) - DC_I}]. \tag{3.17}$$

Spectral analysis of the demodulated time-variant chest wall movement $x(t)$ was performed to extract two prominent spikes: respiration (low frequency but high amplitude in chest wall movement), and heartbeat (high frequency but low amplitude in chest wall movement). Two band-pass filters with known knowledge of the normal respiration and heartbeat frequency distributions were applied to extract both signals simultaneously (for respiration detection, the BPF was set between 0.05 Hz and 0.5 Hz, and for heartbeat detection, the frequency range was set between 0.5 Hz and 2.5 Hz). Therefore, these BPFs covered ranges of 330 respirations per minute (RPM) and 30150 beats per minute (BPM). The breath and heart rates were determined based on the maximal peak derived from fast Fourier transform by using the Hanning window, and were rounded to the nearest integer to represent the estimated breath and heart rates.

3.4 ℓ_1 Minimization with LMI Relaxation to Solve the Elliptic Fitting Problem

3.4.1 Preliminary: Model Parameters Identification

There are five unknowns in the radar signal model, (A_I, A_Q, ϕ_0, DC_I and DC_Q). There are two potential methods to identify these unknowns. The first method is based on statistical machine learning [Bis06]. Given a set of labeled inputs, $x(t)$, statistical learning can build up the relationship between unknowns in the model and input signals. When the relationship model is established, it can estimate the values of unknowns with any arbitrary input, $x(t)$. Unfortunately, this method will fail in this application because the Doppler radar signal model is time-varying and non-stationary, which conflicts with the precondition of most of machine learning methods [RW06]. The second method estimates model parameters based on the signal model Eq. (3.5) and Eq. (3.6) with partial pre-calibration. It is assumed that a prior calibration can be performed on the system such that gain imbalance (the ratio of A_I and A_Q) is 1 and phase imbalance (ϕ_0) is 0. Therefore, the I/Q channel signals will become:

$$I(t) = A_0 \cos(\frac{4\pi x(t)}{\lambda}) + DC_I, \tag{3.18}$$

$$Q(t) = A_0 \sin(\frac{4\pi x(t)}{\lambda}) + DC_Q. \tag{3.19}$$

In this form, there are only three parameters, A_0, DC_I and DC_Q. Note that pairwise samples, $I(n)$ and $Q(n)$, will stay on a circle whose center is (DC_I, DC_Q) and radius is A_0 because

$$(I(t) - DC_I)^2 + (Q(t) - DC_Q)^2 = {A_0}^2. \tag{3.20}$$

It is feasible to fit all samples on a circle via least squares optimization [ZRV12] and then identify these three unknowns. However, this method is not suitable for automated monitoring applications since it requires calibration of gain/phase imbalance. It is impossible to have a pre-fixed calibration for perfect imbalance compensation in practice.

3.4.2 ℓ_2 Minimization Based Fitting

In this work, we attempt to build up the I/Q signal model directly from Eq. (3.5) and (3.6) and demodulate the phase accurately without precalibration.

Given a set of n measurements (I_1, Q_1), (I_2, Q_2), ..., (I_n, Q_n), there is an ellipse:

$$\begin{aligned} \underset{A\sim G}{\arg\min} \quad & \textstyle\sum_{i=1}^{n} \|F(I_i, Q_i, A \sim G)\|_2^2 \\ s.t. \quad & B^2 - 4AC < 0 \end{aligned} \tag{3.21}$$

where the function $F(x, y, A \sim G)$ is defined as the algebraic distance of a point (x, y) to an ellipse parameterized by $A \sim G$.

With the result from Eq. (3.21), we can use Eq. (3.9) - (3.13) to calculate the five parameters in the signal model from the values of $A \sim G$.

We can see that Eq. (3.21) is in a form of quadratically constrained least squares (min-ℓ_2). In general, it is a NP-hard problem [BV04] and impossible to obtain the global optimal solution. Fitzgibbon et al. [FPF99] transferred the quadratic inequality constraint, $B^2 - 4AC < 0$, into an equality constraint, $4AC - B^2 = 1$, under the assumption that all the points (x, y) are close to an ellipse and all distances $F(x, y)$ are close to zeros:

$$\begin{aligned} \underset{A\sim G}{\arg\min} \quad & \textstyle\sum_{i=1}^{n} \|F(I_i, Q_i, A \sim G)\|_2^2 \\ s.t. \quad & 4AC - B^2 = 1. \end{aligned} \tag{3.22}$$

In this way, the formulation in Eq. (3.22) is well-posed and can be solved by

Lagrange regularization and eigenvalue decomposition [FPF99]. There are also some research work under the similar assumption above [HF98,SCH12]. However, this method will suffer from the actual scattered data for two reasons. Firstly, when data is noisy and $F(x, y, A \sim G)$ is relatively large, the equality constraint in Eq. (3.22) will not be equivalent to the inequality constraint in Eq. (3.21). Secondly, it is well-known that ℓ_2 minimization based fitting is sensitive to outlier or sparse measurement errors.

According to compressed sensing theory [Don04] developed in recent years, there are miscellaneous applications indicating that min-ℓ_1 based fitting is more robust to outliers or errors than min-ℓ_2 based fitting [CRT06, WYG09, XZS12]. Inspired by this, we consider using min-ℓ_1 for signal model identification as follows:

$$\begin{aligned} \arg\min_{A\sim G} \quad & \textstyle\sum_{i=1}^{n} |a_i A + b_i B + c_i C + d_i D + e_i E + G| \\ s.t. \quad & B^2 - 4AC < 0. \end{aligned} \tag{3.23}$$

Eq. (3.23) is an ℓ_1 minimization problem with a non-linear constraint and even harder than the quadratically constrained least square problems in Eq. (3.21).

3.4.3 Lower-bound and Linear Matrix Inequality (LMI) Relaxation

In this section, we introduce the method to solve Eq. (3.23) by lower-bound and linear matrix inequality (LMI) relaxation. There are two relaxation steps to solve Eq. (3.23). Firstly, we use the upper bound relaxation to change the objective function. By defining an upper bound distance t_i for each sample (I_i, Q_i), (i.e., $|F(I_i, Q_i, A \sim G)| \leq t_i$), we can have the problem with a linear objective function:

$$
\begin{aligned}
\underset{A\sim G,\mathbf{t}}{\arg\min} \quad & \textstyle\sum_{i=1}^{n} t_i \\
s.t. \quad & F(I_i, Q_i, A \sim G) \leq t_i, \\
& -F(I_i, Q_i, A \sim G) \leq t_i, \\
& t_i \geq 0, i = 1, \cdots, n \\
& B^2 - 4AC < 0.
\end{aligned}
\tag{3.24}
$$

By now, the new problem formulation in Eq. (3.24) is still a non-convex problem and unsolvable. Here we apply LMI relaxation by adding a couple of lifting variables and constraints. More specifically, let $v = [1, A, B, C, D, E, G]^T$ be a basis to build a moment matric, M, by $v \times v^T \succeq 0$:

$$
\begin{aligned}
M &= \begin{bmatrix}
1 & A & B & C & D & E & G \\
A & A^2 & AB & AC & AD & AE & AG \\
B & AB & B^2 & BC & BD & BE & BG \\
C & AC & BC & C^2 & CD & CE & CG \\
D & AD & BD & CD & D^2 & DE & DG \\
E & AE & BE & CE & DE & E^2 & EG \\
G & AG & BG & CG & DG & EG & G^2
\end{bmatrix} \\
&= \begin{bmatrix}
1 & y_1 & y_2 & y_3 & y_4 & y_5 & y_6 \\
y_1 & y_{11} & y_{12} & y_{13} & y_{14} & y_{15} & y_{16} \\
y_2 & y_{12} & y_{22} & y_{23} & y_{24} & y_{25} & y_{26} \\
y_3 & y_{13} & y_{23} & y_{33} & y_{34} & y_{35} & y_{36} \\
y_4 & y_{14} & y_{24} & y_{34} & y_{44} & y_{45} & y_{46} \\
y_5 & y_{15} & y_{25} & y_{35} & y_{45} & y_{55} & y_{56} \\
y_6 & y_{16} & y_{26} & y_{36} & y_{46} & y_{56} & y_{66}
\end{bmatrix} \succeq 0,
\end{aligned}
\tag{3.25}
$$

where

$$
\begin{aligned}
y_1 = A, y_2 = B, y_3 = C, y_4 = D, y_5 = E, \\
y_6 = G, \cdots, y_{22} = B^2, \cdots, y_{13} = AC, \cdots.
\end{aligned}
\tag{3.26}
$$

Note that a 48×1 unknown, $\mathbf{y}$, and a linear matrix inequality constraint, $M \succeq 0$, are introduced here. As a consequence, we can rewrite the formulation in Eq. (3.24) as:

$$
\begin{aligned}
\underset{\mathbf{y},\mathbf{t}}{\arg\min} \quad & \textstyle\sum_{i=1}^{n} t_i \\
s.t. \quad & F(I_i, Q_i, y_1 \sim y_6) \leq t_i, \\
& -F(I_i, Q_i, y_1 \sim y_6) \leq -t_i, \\
& t_i \geq 0, i = 1, \cdots, n \\
& y_{22} - 4y_{13} < 0 \\
& M \succeq 0.
\end{aligned}
\tag{3.27}
$$

Note that the moment matrix M is symmetric and positive semidefinite, and the formulation in Eq. (3.27) is convex and can be solved by semi-definite programming [BV04]. Therefore, we have a feasible solution to identify the signal model with the five unknown parameters.

3.5 Evaluation

Experimental sets were designed to validate the performance of the system. First, an actuator was employed as a controlled subject for a movement measurement test. Second, a pilot study was conducted on 15 subjects to measure vital signs, including heart and respiratory rates. Third, ℓ_1 minimization with LMI relaxation was confirmed to be more robust than ℓ_2 minimization with environmental noise when using simulated data as a test bench.

3.5.1 Evaluation of the Self-calibration Function in a Controlled Environment

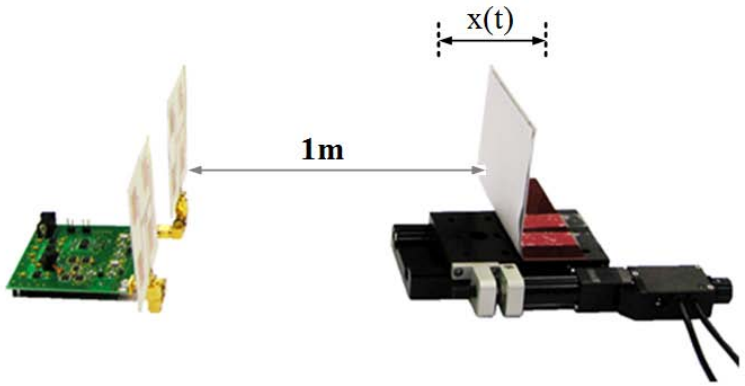

Figure 3.5: Experiment setup for measuring the movement of a controlled actuator

The performance of the noncontact radar sensing system was tested in this experiment. To evaluate the accuracy of the proposed system, a programmable actuator was used to provide controlled motions. As shown in Figure 3.5, a linear actuator (ZABER TNA08A50) and a linear translational stage (ZABER TSB28-1) were placed 1 m from the Doppler-radar motion-sensing system. The actuator was programmed to perform a series of standard sinusoidal movements, and the radar system measured and demodulated the actuator motion. To mimic the chest wall movement (by imitating the respiration and heartbeat of humans), an actuator was programmed to perform a simple harmonic back-and-forth motion toward the fixed position radar. The minimal and maximal displacement was set from 0.1 cm to 4 cm, and the movement frequency changed from 0.2 Hz to 2Hz [GWC97, RS89]. The normalized root mean squared (NRMS) error was used to quantify the measurement error.

$$NRMS = \frac{\sum_{i=1}^{n} dist(i)}{n \cdot A}, \tag{3.28}$$

where $dist(i)$ is the distance from the measured point to the sinusoidal curve, and

A is the amplitude of movements.

The measured motion was consistent with the presetup harmonic motion of the linear actuator, and the RMS error was less than 1%. To clearly represent the residual change that occurred when using different magnitudes and frequencies, the results are plotted in Figure 3.6. Based on this figure, the average measurement error of the Doppler radar sensing system was less than 3%. This indicates that the measurement error was uncorrelated with movement frequency (in this frequency range) but strongly associated with the movement magnitude: the larger the amplitude of motion, the smaller the measurement error was.

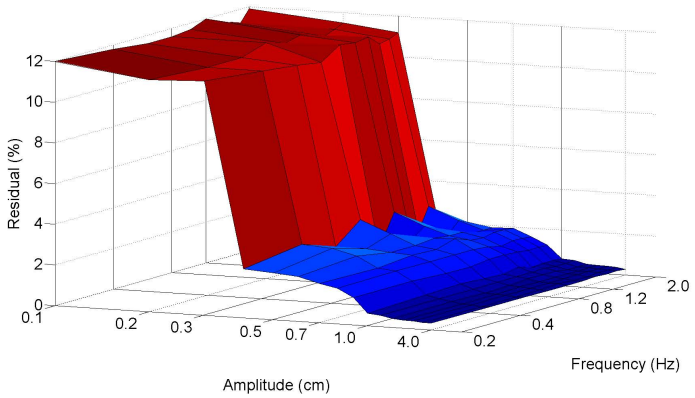

Figure 3.6: The residual surface of sinusoidal actuator movement measurement with variations in amplitude and frequency.

To demonstrate the benefits of self-calibration, the same experiment was conducted in three environments: a lab environment (results presented previously), an outdoor environment, and a corridor on campus. The radar system was initially set up in the lab environment and then moved to the other two locations. These two locations were randomly chosen to demonstrate the portability of a self-calibrating radar. The results in Table 3.2 demonstrate the superiority of this proposed modeling layer process. Without enabling self-calibration, when the operating environment changed from the initial location, the NRMS error increased. However, when enabling self-calibration, the RMS error remained less than 1%.

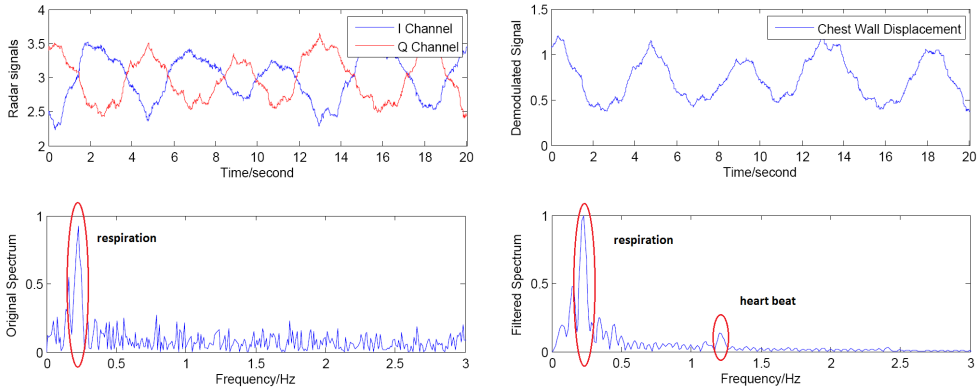

Figure 3.7: Comparison of raw and demodulated signals and their respective spectrum analysis for extracting respiration and heartbeat signals

The highest error occurred in the corridor environment because numerous factors cause multipath radar transmission in the long, narrow hallway. Although the proposed methods can be used to calculate radar parameters in real time, manual calibration performed more favorably. According to Table 3.2, manually precalibrating the radar in a lab environment was more effective than using the proposed method. This is because self-calibrated parameters always override a preset default and manual calibration is typically more efficient than fitting-based methods. Therefore, if a radar system must be operated to measure distance with high accuracy, then manual calibration may still be required. However, the relatively slow and periodic respiration and heartbeat signals that are identified are not required to exhibit exact chest-movement displacement. Instead, extracting the periodic changes is more critical than determining the absolute distances. Furthermore, using a radar that is adaptable to various environments is desirable.

3.5.2 Human Vital-Signs Monitoring with 15 Subjects

Human vital signs derived from radar modulated signals were measured in this experiment. Fifteen subjects were recruited and each subject sat in front of the Doppler radar sensor in a lab environment, as shown in Figure 3.8. The distance

Table 3.2: Error estimation of the radar measurement under three different environment

NRMS(%)	Lab Env	Outdoor	Corridor
with Self-calibration	0.78	0.87	0.92
w/o Self-calibration	0.72	6.21	9.43

Figure 3.8: The Doppler radar measures vital signs from a subject.

between the subject and the radar sensor varied according to the person. When using the self-calibrating mechanism, tuning the radar for each subject was unnecessary. Each measurement lasted for 120 s, and each subject was tested 3 times. To obtain the breath rate ground truth, a video camera was used to record the chest wall movement and QPS ECG sensor [Car] waveform, and the number of breaths and heartbeats were counted manually within 120 s. Figure 3.7 shows the radar measurements and demodulation results for one subject analyzed using the noncontact vital sign measurement system. Both the raw and demodulated data were visualized. A substantial gain imbalance in I/Q signals was observed. Spectral analysis was applied to extract respiration and heartbeat signals. To validate the necessity of the signal-processing method, spectral analysis of the raw radar signal was conducted. In this figure, the Q channel with a phase similar to the demodulated chest wall displacement was chosen. The frequency components

of respiration and heartbeat were prominent in the demodulated data spectrum. The demodulated signals were compared with the respiration and heartbeat movements of the subject and were determined to be matched with the ground truth data. The detailed characteristics of the 15 subjects are presented in Table 3.3. Respiration was measured using RPM and heartbeat was measured using BPM.

Both respiration and heartbeat signals were extracted and identified using spectral analysis. As shown in Figure 3.7, extracting these signals from raw data is difficult. Although respiration can be identified within a range of frequencies (the largest peak in the figure is wider than the other peaks), the heartbeat signal was barely identifiable. In addition, the amplitude of the peak of respiration was much smaller than the spectrum of the demodulated displacement. Voltage rather than centimeters was used to represent the displacement because the radar was not used to measure precise chest wall displacement; instead, the periodic phenomenon of the displacement was identified.

3.5.3 Empirical Comparison Between ℓ_1 Minimization with LMI Relaxation and ℓ_2 Elliptic Fitting

A simulated data set was developed to quantify the performance of the proposed demodulation method. The data set was simulated using known ellipses with noise and outliers. Specifically, the simulated dataset was divided into two classes. One class comprised the simulated data with outliers, and the distance from the outliers to the ellipse ranged up to 50% of the semimajor axis. The other class comprised simulated data with noise, for which the signal-to-noise ratio (SNR) varied from 0.01 to 0.5. In the experiment, the proposed algorithm was applied to perform ellipse fitting on the test bench. The Fitzgibbon ℓ_2 minimization method [FPF99] was used for comparison. First, the performance of the algorithm when using the outlier data set was evaluated. Figure 3.9(a) and Figure 3.9(b) show an example of ellipse fitting using the traditional ℓ_2 minimization method and the proposed

ℓ_1 minimization method, respectively. The blue dots represent the clean data (zero offset), the red dots represent the outliers, the black curve is the fitting result, and the red dashed curve is the ground truth. Based on this example (15% outliers), the ℓ_1 based algorithm was robust to the red outliers, and the fitted ellipse matched the clean data (Figure 3.9(b)). By contrast, the ℓ_2 based method was affected by the outlier points, and an obvious mismatch existed between the fitted ellipse and the ground truth (Figure 3.9(a)).

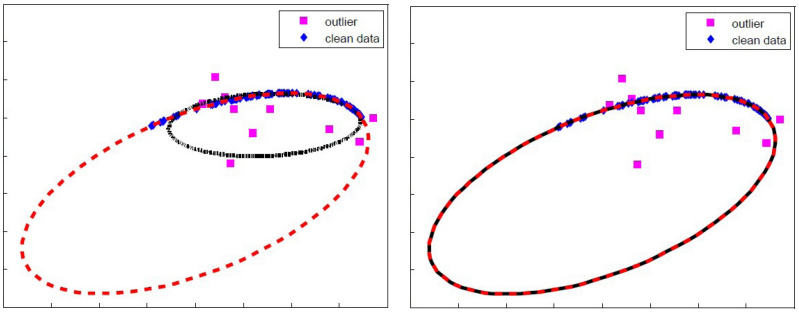

(a) ℓ_2 based method (b) ℓ_1 based method

Figure 3.9: An example of the fitting results on outlier dataset for both algorithms. The outlier percentage is 15% and SNR=20.

Both methods with different outlier percentages, ranging from 5% to 40%, were also evaluated. For simplicity, the overlap area between the fitted ellipse and ground-truth ellipse was used to evaluate the matching accuracy [HC11]. Figure 3.10 illustrates two accuracy curves corresponding to these two strategies, and shows that the ℓ_2-based method was sensitive to outliers, whereas the ℓ_1 based method tolerated up to 20% of the outliers.

Second, the performance of the proposed system was tested using a set of data containing Gaussian noise. Figure 3.11 illustrates the stability of the ℓ_1 and ℓ_2 algorithms with noise. The SNR ranged from 10 to 100. As the noise levels increased, the deviation from the ground truth for both the algorithms increased (the red ellipse). However, ℓ_1 was still more favorable than ℓ_2 at all SNR levels.

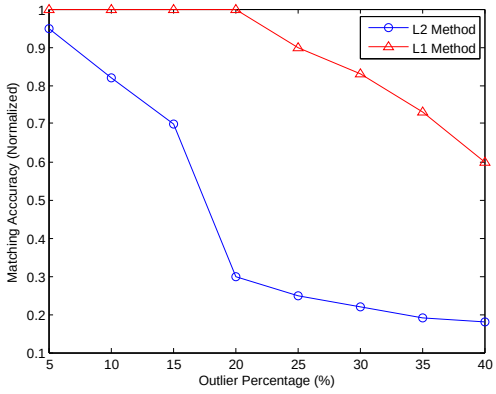

Figure 3.10: Two matching accuracy changing curves with different outlier percentages use ℓ_1 based method versus ℓ_2 based method.

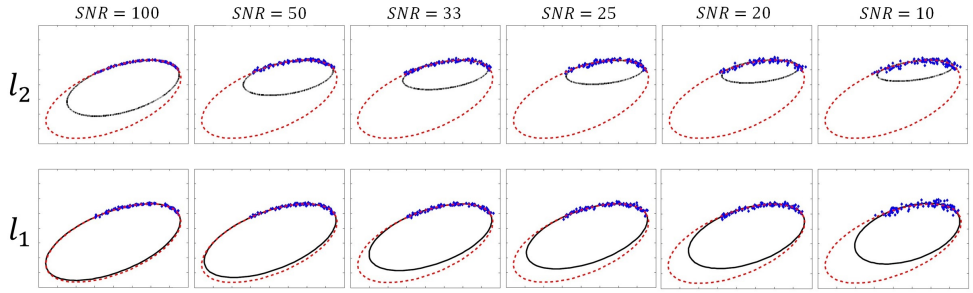

Figure 3.11: Fitting results on noisy dataset for two algorithms. SNR ranges from 10 to 100. The first row (from (a) to (f)) is the fitting results of the ℓ_2 based method, and the second row (from (g) to (l)) is the fitting results of the ℓ_1 based method. In each figure, the red dashed curve is the ground truth and the black solid curve is the fitted curve.

Table 3.3: 15 subjects' respiration and heartbeat extraction compare with the ground truth.

Personal Info			Ground Truth			Extracted Data			Error Per Trail		
Sex(M/F)	Height(inch)	Weight(lbs)	Trial1	Trial2	Trial3	Trial1	Trial2	Trial3	Trial1	Trial2	Trial3
M	67	173	18/72	19/72	18/72	18/72	19/73	18/72	0/0	0/**1**	0/0
M	67	156	15/66	15/66	16/65	15/66	15/65	16/65	0/0	0/**1**	0/0
M	75	165	17/71	17/72	17/70	17/71	17/72	17/70	0/0	0/0	0/0
M	73	182	19/68	19/69	18/67	19/68	20/69	18/67	0/0	**1**/0	0/0
M	66	176	14/80	13/82	15/80	14/80	14/81	13/79	0/0	**1**/**1**	**2**/**1**
F	63	102	20/84	19/84	20/85	20/84	19/84	20/85	0/0	0/0	0/0
M	65	160	17/75	17/76	18/76	18/75	17/76	18/76	**1**/0	0/0	0/0
F	65	108	15/82	15/82	15/82	15/81	16/82	15/82	0/**1**	**1**/0	0/0
M	70	140	12/75	12/75	12/75	12/76	12/75	13/75	0/**1**	0/0	**1**/0
M	72	167	18/80	18/79	17/79	18/80	18/79	17/80	0/0	0/0	0/**1**
M	69	143	16/63	16/63	17/64	16/63	16/63	17/64	0/0	0/0	0/0
M	68	190	19/68	19/69	18/68	17/68	19/69	18/68	**2**/0	0/0	0/0
M	68	150	13/74	13/74	13/74	13/74	13/74	12/75	0/0	0/0	**1**/**1**
M	70	178	15/70	15/70	16/71	15/70	15/70	16/71	0/0	0/0	0/0
F	65	112	17/82	17/82	17/83	17/82	17/82	18/83	0/0	0/0	**1**/0
Averaged by number of breath: 17/min and number of heartbeat: 75/min									1.18/0.17	1.18/0.27	1.76/0.27

3.6 Conclusion

Vital signs (i.e., heartbeat and respiration) are crucial physiological signals that are useful in numerous medical applications. The process of measuring these signals should be simple, reliable, and comfortable for patients. In this paper, a noncontact self-calibrating vital signal monitoring system based on the Doppler radar is presented. The system hardware and software were designed with a four-tiered layer structure. To enable accurate vital-sign measurement, baseband signals in the radar sensor were modeled and a framework for signal demodulation was proposed. Specifically, a signal model identification method was formulated into a quadratically constrained ℓ_1 minimization problem and solved using the upper bound and linear matrix inequality (LMI) relaxations. The performance of the proposed system was comprehensively evaluated using three experimental sets, and the results indicated that this system can be used to effectively measure human vital signs.

CHAPTER 4

Augmented Visualization

4.1 Introduction

Excessive ultraviolet radiation is an important issue in skin healthcare. Overdosed ultraviolet exposure can lead to sunburn and even skin cancer, the most common type of cancer in the United States [fac]. One in five Americans develops skin cancer in lifetime [Rob05], more than incidences of 3.5 million skin cancer diagnoses annually [RWH10]. According to a report [HFW03], skin cancer is also the most costly of all cancers to treat.

Figure 4.1: UV sensing and visualization system prototype.

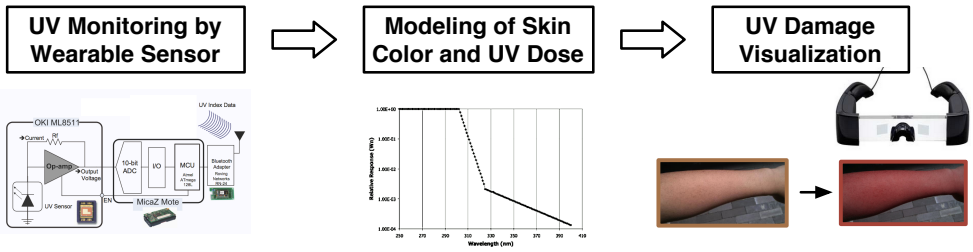

Figure 4.2: Three components in the UV sensing and visualization system: UV sensor, UV-Skin modeling, and Damage visualization.

Overexposure to sun radiation, especially within the ultraviolet region of the spectrum, is the predominant risk factor for the development of skin cancer [HM-C04]. While a moderate amount of sunlight is helpful to synthesize vitamin D, excessive UV radiation exposure can increase the chance of skin cancer and cause severe eye injuries. A field study [HGR94] investigated UV exposure of six different outdoor activities (Tennis, Sailing, Swimming, Walking, Golfing and Gardening) in seven anatomical sites over two consecutive days. The result of high amount of UV exposure verified the necessity to monitor UV radiation during outdoor activities in order to avoid skin and eye damage.

The effect of UV exposure can first darken and tan [tan] surface skin. When UV radiation is abundant, The skin cells in the top layer, Epidermis, efficiently produce melanin, a pigment giving skin its natural color. Therefore, skin color change caused by sunburn is widely used as an indicator of the degree of UV exposure. Unfortunately, it is always too late to apply protection when overexposured. Therefore, a UV real-time monitoring and warning system is desirable to notify users before they get sunburned.

In this paper, we present the design of a wearable UV sensing and visualization system for outdoor skin protection, as shown in Figure 4.1. There are three main components in the system. UV radiation monitoring and recording are the first component. UV index is a commonly accepted parameter for measuring UV

radiation intensity. Our system uses ML8511 UV sensors to monitor UV index and record the monitoring results. Since the damage caused by UV is accumulated over days, the sensor data should be stored in order to make personalized skin care suggestions. These data can be also sent to doctors for receiving analysis and feedback. In addition, a skin color model based on four different skin types was built. We refer preliminary knowledge about human skin to develop the ultraviolet responsive color model of skin. Thus we can predict and show users the sunburn visual effects on a variety of skin types. Finally, participants wear AR glasses in order to see augmented sunburn effects on their body parts. Our visualization deliberately over-amplifies the effect of overexposure to better warn users the consequence of overexposure.

4.2 Related Work

There are two types of UV monitoring products in the market. The first type records accurate measurement with a personal UV meter. The second type provides a visual warning to users by using a paper wrist strap which will change color under high UV index.

Personal UV meters [met] are normally designed as accessories on bag or clothes. Some of them may have small screens to display the current UV index. The advanced ones can directly connect to computers to exchange recorded daily UV data. These UV meters let users know a real-time UV index in current location. The measurement is more accurate than a weather report, which only provides hourly forecast in a large area. However, the UV meter is not visually convincing. The best visualization it can achieve is to display a UV index on a small screen. However, users have little idea about what the UV index means and how serious the damage will be.

A commercial available product uses a paper wrist strap [wri] to warn users

by visual effect. It changes color with UV index so that users will be notified when the UV index is high. However, it is disposable and becomes non-resuable once triggered by high UV index. Thus users have to prepare several wrist straps, which can be inconvenient. Moreover, it can neither provide accurate UV data, nor record daily UV dose for long term analysis.

These attempts confirm the need of an effective personalized UV monitoring and visual notification system. They inspire us to come up with a new system which can monitor UV dose by wearable sensors, analyze with skin model, and exaggerate sunburn effect to notify users to apply protection, such as sunscreen.

4.3 Design Overview

Our system, as shown in Figure 4.2, monitors UV index from sensors, calculates effective UV dose based on skin model, and finally visualizes UV effects to warn users. The UV sensitive sensor only provides output voltage corresponding to UV intensity; thus we have to first derive UV index from the output voltage. Then, the system accumulates UV radiation information to calculate the effective dose of UV. After users enter their personal skin information, our system can choose a proper skin model for the user. With personalized skin model, our system can better estimate possible sunburn effective skin color. Finally, AR glass visualizes over-amplified sunburn on the skin in order to warn the user. The following sections provide more system design detail in hardware, modeling and visualization.

4.4 UV Monitoring and Visualization System

In this section, we discuss the hardware design of our personalized UV monitoring and visualization system. The system structure is shown in Figure 4.3. In our

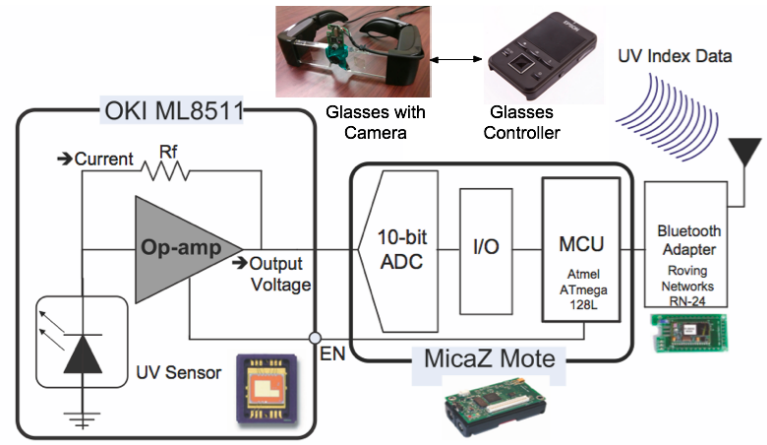

Figure 4.3: Hardware design diagram.

design, the system consists of three main parts: a wearable UV sensing system, a skin color computational model and a UV effect visualization glasses. Firstly, the sensor measures UV intensity and computes UV index. When a Bluetooth adapter sends UV data from sensors to an AR glasses controller, the computational model can predict the UV effect on the skin. In the end, our system augments the results on the AR glasses for users. In the following part, we will introduce hardware components in detail.

4.4.1 UV Sensor System

We collect UV data using portable sensors with controlling and wireless transmission system.

The ML8511 sensor in Figure 4.4 is a photo diode that measures UV intensity by thin-film Silicon-On-Insulator (SOI) Technology. The additional filter further improves the accordance with the erythema action spectrum curve of the human skin. Its current-to-voltage conversion amplifier is comprised of an operational amplifier and a resistor, which provides output voltage proportional to electrical current value. The output voltage can be sent directly to the analog-to-digital

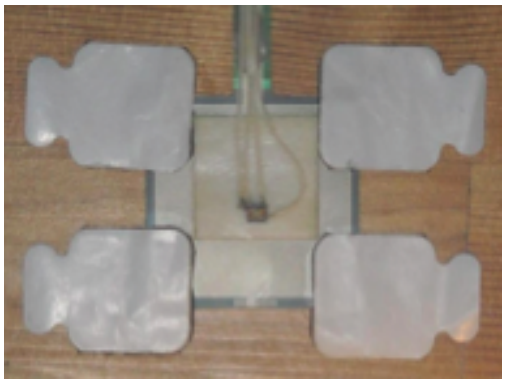

Figure 4.4: ML8511 UV sensor on a patch.

Sensor output voltage	ADC output	UV index
0.993	320-345	0
1.073	345-370	1
1.153	370-395	2
1.233	395-420	3
1.313	420-445	4
1.393	445-470	5
1.473	470-495	6
1.553	495-520	7
1.633	520-545	8
1.713	545-570	9
1.793	570-595	10
1.873	595-620	11
1.953	620-645	12
2.033	645-670	13
2.113	670-695	14
2.193	695-720	15
2.273	720-745	16
2.353	745-770	17
2.433	770-795	18
2.513	795-820	19
2.593	820-845	20

Table 4.1: UV indices correspond to the sensor and ADC outputs (Vcc=3.0V).

converter (ADC), where the voltage is converted into a digital signal. The resulting digital signal is processed by the Atmel ATmega128 microcontroller to lookup the

current UV index from Table 4.1. Finally, it sends UV index data to the RN-24 Bluetooth adapter every 15 seconds.

Figure 4.5 shows the spectral sensitivity characteristics of the photo diode in ML8511. Due to its SOI structure, this silicon photo diode is highly sensitive and selective only in the UV-A (320 to 400 nm wavelengths) and UV-B (280 to 320 nm wavelengths). This property is useful in our UV measurement, as UV-A and UV-B are the UV radiations which do damage to the human skin. The sensor producer also takes different wavelength's spectral sensitivity into account, thus providing output voltage after correction.

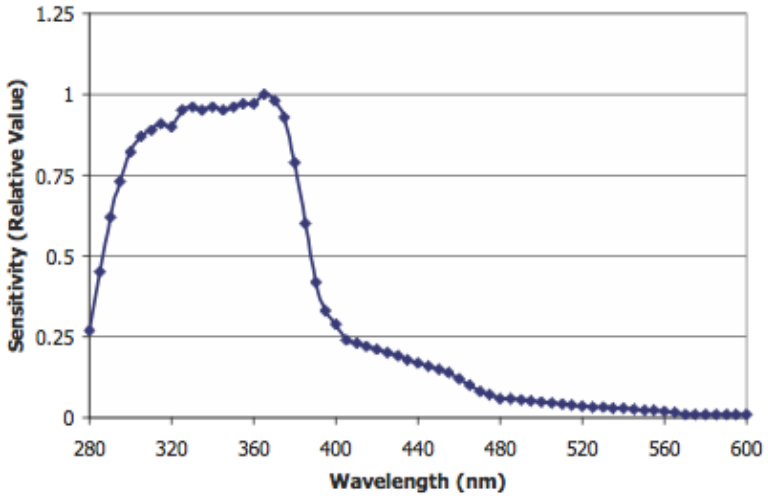

Figure 4.5: Spectral sensitivity characteristics of ML8511. It is highly sensitive and selective to UV-A and UV-B.

The calculation of the UV index is: UVI $= \lceil (ADC - 320)/5 \rceil * 0.2$. In the darkness, the sensor output is 0.993V and ADC output is 320. Therefore, we should subtract 320 from the current ADC output and scale it. This equation determines that our UV index calculation precision is 0.2 unit.

Furthermore, we should consider the effect of incidence angle. If the sunshine is not vertical to the sensor, the UV measurement will be less than the real value. According to our experiment Table 4.2, we find the incidence angle less than 20

Table 4.2: Sensor output for different incidence angles.

Incidence angle	Sensor output voltage	ADC output	Corresponding UV index
0°	1.811	574	10.0
20°	1.731	550	9.2
45°	1.473	472	6.8

degree is acceptable. As a result, we put two UV sensors on the user and take the largest measurement value of the measurements.

4.4.2 Augmented Reality Glass

The visualization part is made possible by an augmented reality glasses. In our system prototype, we choose Epson Moverio BT-100, a light-weighted augmented reality glasses shown in Figure 4.6. This pair of AR glasses has see-through display for each eye; thus we can display a sunburn effect layer on top of the skin. Its head display connects with a controller running Android system. Thus, it is easier to develop our client app and later port to other hardwares also running Android system. Moreover, a head mounted camera is necessary to fetch the user's skin image and then visualize the UV effect. As the glasses is not equipped with a camera, we add a CMOS Camera Module (resolution 728x488) which connects with the glasses controller. The user can touch the trackpad on the controller to interact with the glasses. In the future system implementation, we aim to take advantage of the lighter, more wearable Google Glass for better wearing experience.

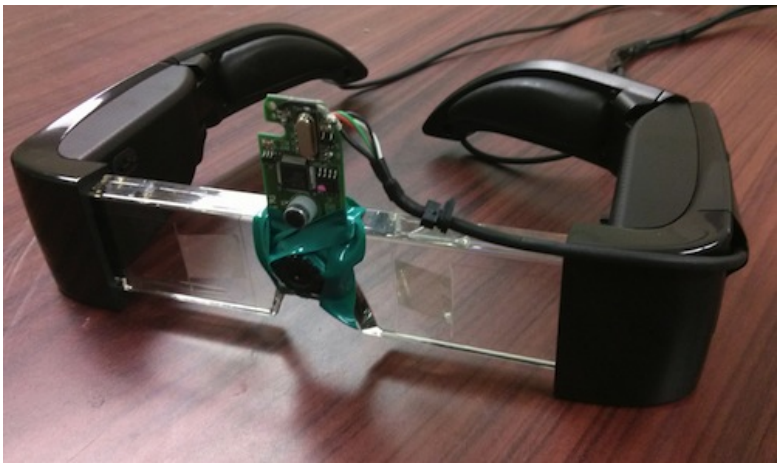

Figure 4.6: Epson Moverio BT-100 AR glass with a camera.

4.5 Skin Modeling and Visualization

The glasses controller receives UV index data via Bluetooth. According to the user skin model, the client app processes UV index data and generates an AR layer of sunburn effect visualization on the skin. Thus, the user can be warned to take sunburn protection in time.

4.5.1 Modeling

In order to predict and visualize the sunburn effect on skin, we need preliminary knowledge about human skin, and then develop the ultraviolet responsive color model of skin.

4.5.1.1 Damaging UV Radiant Flux Calculation

We calculate damaging UV radiant flux based on McKinlay-Diffey erythema action spectrum curve shown in Figure 4.7. The calculations are weighted in favor of the most sensitive UV wavelengths to human skin. We derive the UV index by integrating human body erythema action spectrum and the intensity of solar UV radiation at different wavelengths.

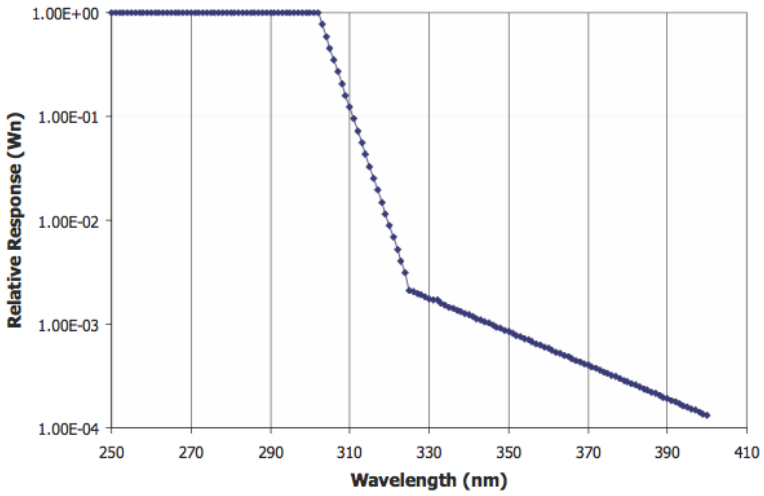

Figure 4.7: McKinlay-Diffey Erythema action spectrum.

As seen in McKinlay-Diffey erythema action spectrum curve, skin damage due to sun exposure is dependent on wavelength over the UV range (295 to 325 nm), as the shorter wavelength can cause around 30 times damage of the longer one's.

$$\text{UV dose} = \int_0^T \int_{190}^{400} W_{\text{n}} * E_\lambda d\lambda dt$$

This equation calculates the effective dose of UV in general form. To get the effective irradiance, we integrate the multiplication of weighting of the erythema action spectrum (W_n) and the solar spectral irradiance radiated on the surface (E_λ) in the UV radiation hazard bandwidth (190 to 400 nm). The time integral of the effective irradiance is called effective dose; the unit of effective dose is W/m^2.

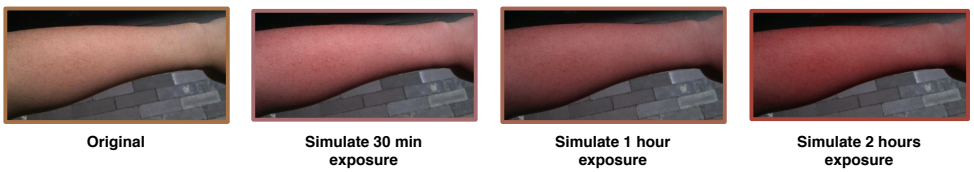

Figure 4.8: Normal arm skin color and the sunburn effect visualization after 30 mins, 1 hour, and 2 hours.

The studies of the erythemal influence are frequently based on the minimum dose of UV erythemal radiation, which can produce a noticeable reddening on

human skin. This dose is known as the MED (minimum erythemal dose) and is always related to a specific skin type. If the UV irradiance is 1 MED/hour, it should take an hour to receive the minimum erythemal dose when a person is exposed to this irradiance. 1 MED corresponds to a total dose of 210 J/m^2. Thus 1 MED/hour = (210 J/m^2)/3600 s = 58.3 mW/m^2 = 2.33 UVI.

4.5.1.2 Skin Type

People with different skin types skin react differently towards UV exposure. At present, the majority of countries has adopted four skin types for tanning capacity, on the basis of COST-713 [713] recommendations. The principal characteristics of these skin types indicate the tolerable MEDs and maximum exposure time per UVI, which are defined by the DIN 5050 standard in Table 4.3.

For example, an unprotected type 3 skin person will start to have sunburn in just 20 minutes, under UVI 10 sun exposure: [200 (min) / 10 (UVI) = 20 min]. If the same person uses an SPF 30 sunscreen, the time will be extended to 600 minutes, or 10 hours: [20 (min) x 30 (SPF) = 600 min].

Table 4.3: Skin types with the corresponding tolerated MEDs and the maximum exposure time.

Color, burning and tanning in the sun	Tolerable MEDs	Max exposure
White, always burns, never tans	2 hecto J/m2	67 min/UVI
Yellow, usually burns, sometimes tans	4 hecto J/m2	100 min/UVI
Yellow, sometimes burns, usually tans	5.75 hecto J/m2	200 min/UVI
Black, rarely burns, always tans	8.5 hecto J/m2	300 min/UVI

4.5.1.3 Skin Color

Every person has a different response to sunburn, so there exists no model that fits perfectly for everyone. Instead we build models based on four skin types and positive correlation of the dose - response curve.

Based on skin type and UV dose, we can predict when the user will start to sunburn on the skin. Human's skin has two kinds of colors: constitutive and facultative [col]. Constitutive skin color (see the underside of the arm) is the natural, genetically determined color of the epidermis. It is hardly influenced by ultraviolet light or hormone exposure. As the result, our research focuses on facultative skin color which, in contrast, results from exposure to UV light and other environmental factors. Tanning, for instance, changes the composition of melanin in the skin and increases the amount and size of melanin produced by melanocytes. Thus, facultative skin is normally darker than constitutive skin.

In daily life, we assess the level of severity of sunburn damage based on the unusual "redness" we see on the skin. According to medical researches [Lee95], the redness of the skin is increased by UV-induced erythema. Moreover, another research [WEM90] indicated positive correlations between UV dose and increase of redness. Also, in lightly pigmented skin, the dose-response curves were steep, whereas in darkly pigmented skin the curves were much flatter.

4.5.2 Visualization

Based on the skin model, our system can visualize sunburn effect on the user's arm. However, our visualization is not an exact match or perfect prediction of sunburn effect. Our primary goal is to bring caution towards possible outcomes; thus, the visual effect is a bit over-amplified to better warn users.

From our model, we first notice the positive correlations between UV dose and the increase of redness. From experimental data of [WEM90], we approximate

their correlation as linear relationship.

In real life setting, the UV index will change with user's activities. For example, a user may only stay outside for 1 or 2 minutes and then go indoor. Under these circumstances, we should not disturb the user by alerting unnecessary sunburn information. Thus, we use method mentioned before to integrate UV index and UV dose every 5 minutes. Based on average UVI, we can predict how long it will take to sunburn.

In order to analyze skin color and increase redness, we introduce HSV, a commonly chosen color model in computer vision research and application. HSV stands for Hue, Saturation and Value. The Hue channel obtains robustness to lighting changes or removing shadows. This property is useful for us to find and analyze a specific range of color. In this case, using HSV in skin color analysis is better than using the normal RGB color space. During our experiment on participants' normal skin colors, we find the Hue channel ranges from 0 to 43 and 338 to 360 (maximum value 360). We also collect mild sunburn photos, and find the Hue channel ranges from 0 to 12 and 355 to 360. We can see the Hue range in Figure 4.9. In order to present sunburn starting effect, we use a fitting equation to convert Hue channel: $((\text{Hue}_{\text{Sunburned}} + 6) \bmod 360) / 17 = ((\text{Hue}_{\text{Normal}} + 22) \bmod 360) / 67$. We can use this relation to calculate the sunburn effect of Hue of skin.

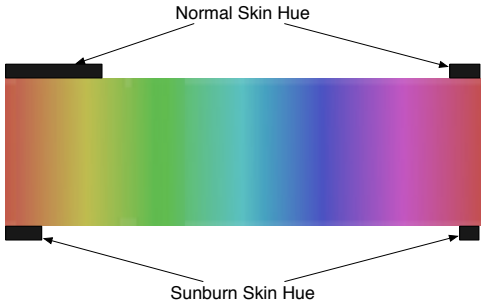

Figure 4.9: Hue range of the normal and sunburned skin.

Mild and heavy sunburn mainly differ from their Value channel, which takes charge of skin brightness. The heavier the sunburn is, the darker the skin is. Thus, from linear correlation of dose-response, we can decrease Value channel by 2% for every 50mJ/cm^2 dose.

Figure 4.8 is an example of sunburn warning effect. The normal arm is near yellow-brown. When we apply the fitting equation on Hue channel, the arm turns out to be red and similar to mild sunburn. After this, we decrease Value channel based on a UV dose to show different levels of sunburn during different time periods under this UV.

After the user sees sunburn effect layer, our system provides detailed information in case the user hopes to learn more to take protective actions.

4.6 Evaluation

After implementing our system, we evaluate the system with participants for feedback and design improvement suggestion. A total of 9 healthy UCLA undergraduates took part in the experiment. Before the experiment, we debriefed our procedure to participants. We also told them that we would only collect UV data from sensors, without recording any private information from our camera.

Participants' personal information is needed to select a proper skin model. As different users have different skin types, their ultraviolet tolerance may also be different. When a user logs on to our system first time, we will ask the user for his/her skin type. The user can look up for skin type from Table 4.3. In order to better monitor UV intake for individual users, we recommend users to confirm their skin information with their doctors.

We encourage users to take sunscreen in order to protect themselves. Thus our model needs to consider SPF (Sun Protection Factor) of sunscreen to better predict the UV effect. Every time a user launches our client app, we will provide

local weather forecasts (from Yahoo! Weather API). Based on the UV index, we will recommend whether the user should use sunscreen and which SPF is necessary. If the user decides to use sunscreen, he/she will need to enter its SPF in our system before he/she uses.

4.6.1 Result Analysis of UV Monitoring

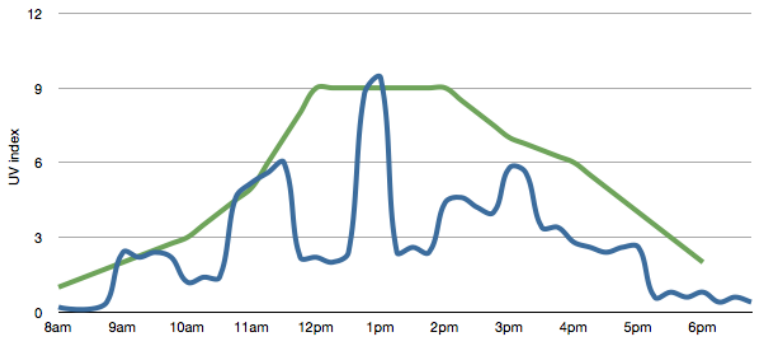

Figure 4.10: UV index monitoring results from the local weather forecast(green) and our wearable sensor(blue).

Figure 4.10 shows UV index monitoring result in one day. The local weather forecast (green line) can best provide an hourly report. In contrast, our sensor makes measurement every 15 seconds. Higher sample rate can provide better measurement of UV dose during user daily activities. Moreover, the forecast curve is an approximate result of outdoor UV index across a large area, so the forecast is not applicable to each person's activity range. Most importantly, as we can see in the plot, the user may not always stay outside, so the UV index forecast cannot accurately indicate cumulative UV dose. These are the reasons to use wearable UV sensor.

4.6.2 User Experience of Visualization

We asked each participant to wear our system for two days and give us their feedback. During the first day, we only equipped our UV sensor on the user's arm and allowed him/her to check the UV index on our website. We sent a questionnaire to the user for feedback at the end of that day. On the next day, we provided AR glasses to the user for the visualization functionality. At the end of the day, we sent the same questionnaire to the user; thus we can compare the subjective experience with and without visualization.

4.6.2.1 Questionnaire.

(Q1) I can better protect myself under sun with this system.
(Q2) The interface is easy to interact with.
(Q3) The hardware system is heavy and cumbersome.
(Q4) I feel my skin is healthier and less likely to burn.
(Q5) (Only for AR glasses) The visualization is effective to warn me.
(Q6) (Only for AR glasses) The visualization effect disturbs my daily life.
(Q7) (Open Question) It will be great if the system includes this feature:

All these statements were answered with a 9-point Likert scale [Lik32], where 1 = strongly disagree, 3 = disagree, 5 = neither agree nor disagree, 7 = agree, and 9 = strongly agree.

Figure 4.11 shows the average response from participants in both with and without AR glasses settings. We use t-test for a population mean for AR glasses setting. The response without AR glasses is also on the plot for comparison. Our null hypothesis is μ=5, which means that according to our participants' feedback, our visualization system is unlikely to have an obvious positive effect on others. Our alternative hypothesis is μ >5, which means our visualization system has an obvious positive effect on others. For Q6, as the sample mean < 5, our alternative

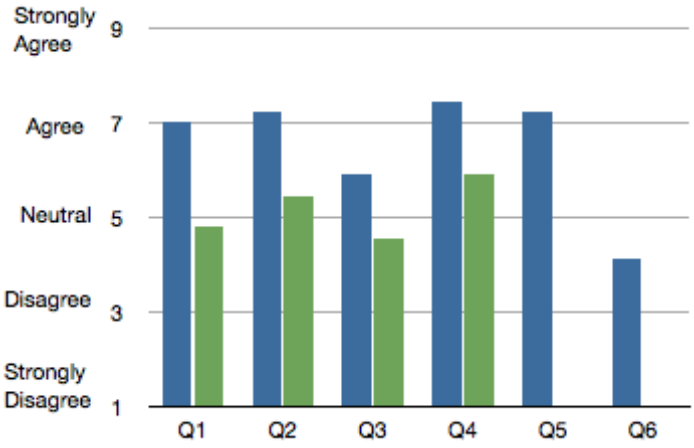

Figure 4.11: The participants' average responses with(blue) and without(green) AR glass settings.

hypothesis turns out to be μ <5. We choose 0.05, an often chosen fixed number, as our significance level.

Q1 (AVG=7, STDEV=1.72, p-value=4.23e-3) reflects the subjective experience in UV protection. We found that the null hypothesis is rejected due to small p-value(much smaller than 0.05), which validates our visualization has a positive impact on UV protection.

Q3 (AVG=5.89, STDEV=1.67, p-value=5.31e-2) reflects users' consideration about the weight of the system. The null hypothesis is not rejected, which indicates that users are not particularly worry about the system weight and understand that the finalized solution will use even lighter AR glasses. However, we can still find p-value is not significantly larger than 0.05, so we need to consider this problem seriously.

Q4 (AVG=7.44, STDEV=1.56, p-value=1.14e-3) reflects the users' feeling of their skin. The null hypothesis is rejected, which indicates that users satisfy with our system to improve their skin health.

Q5 (AVG=7.22, STDEV=1.83, p-value=1.37e-3) rejects the null hypothesis

and validates that visualization is an effective warning notification.

4.7 Conclusion

These days, as the Earth's protective ozone layer gets thinner, ultraviolet (UV) radiation threat is growing. In addition, getting tanned as a fashion leads people to wear less clothing, which increases UV intake. Excessive exposure to ultraviolet will lead to sunburn and even skin cancer. Therefore, neither insufficient nor excessive exposure is desirable. Although there are tons of UV meters on the market, users may have a hard time to understand the unintuitive UV index reading. Thus, there is a potential demand for a portable system which can keep track of users' daily UV exposure dose, visualize possible sunburned consequences, and provide appropriate skin care recommendations. In this paper, we present a personalized UV monitoring and notification system. This system can continuously track UV exposure by wearable UV sensors. It can also visualize the cumulative UV exposure dose according to a predictive sunburned skin color model. Such an augmented skin color can provide a warning message to indicate the possible result of continuous UV exposure. Compared with existing systems, our solution not only allows users to monitor their daily UV exposure, but also provides an unobtrusive UV visualization model which effectively warns users to take appropriate actions to avoid potential skin damage. This system has been tested on 9 subjects, and the evaluation feedback indicates that our system is promising for UV monitoring and sunburn prevention.

CHAPTER 5

Virtual Reality Based Rehabilitation

5.1 Introduction

Frozen shoulder refers to a condition caused by impaired soft tissues and articular capsule of the shoulder. It commonly happens to people aged between 40 and 65 years old and it is more likely to appear in female than males [CBH08]. Frozen shoulder severity can be categorized into four stages: Preadhesive, Adhesive, Maturation, and Chronic. In Preadhesive stage (0-3 months), a fibrinous synovial inflammatory reaction is detectable only by arthroscopy. The patients usually present with signs and symptoms of impingement syndrome. The main complaint is pain and minimum deficit in range of motion is detected. Adhesive stage (4-9 months), the acute synovial inflammation is apparent on physical evaluation. Arthroscopic findings demonstrated that the normal spacing between capsular fold, humeral head and biceps tendon, glenoid and humeral head diminish significantly. The patient experiences severe pain and loss of motion. Patients in Maturation stage (10-15 months) and Chronic stage (16-24 months) are treated as having frozen shoulder problem. These stages are evident by the maturation of the inflammatory process. The dependent fold is only half of its original size and adherence between various structures are formed. Eventually, Capsular adhesions are fully mature and markedly restricted. Clinically, the shoulder is frozen [Bat10].

Patients with frozen shoulder usually accompanied with limitation of range of shoulder motion and pain. Therefore, the goal of treatment is to restore, retain

range of their shoulder motion, muscle strength and alleviate their pains [KKW64]. Using Pandol and antiphlogistic medicine or steroid injection can alleviate pains; however, the effect is very limited for severe frozen shoulder patients. Surgery may be needed for those patients instead, but both medicine or surgery treatments require continuous physical shoulder rehabilitation to retain the original functionality. Common rehabilitation exercises including shoulder joints stretching and rotating exercises, such as Codman's exercise, pulley therapy, finger crawling exercise, and joint mobilization, should be applied to stretch the adhesive capsulitis for retaining original shoulder joint mobility.

In addition, appropriate bridge muscle strength training is also required to prevent muscle atrophy [CCH07a]. Bergmark [PKO03] reports that bridge muscles control the exercise direction of the spinal cord and affect extremities' movement. Bridge muscle maintains the balance of the spinal cord; therefore, it allowed extremities to move, such as shoulders and arms. Appropriate bridge exercises can effectively strength bridge muscle and provide positive effect on frozen shoulder rehabilitation, such as reducing cervical muscle activity and reinforce trunk muscle strength [Sec]. Hodges and Richard [RM11] confirmed that all movements involved upper/lower extremities are followed by bridge muscle shrinks. Therefore, improving muscle strength of the bridge muscle largely affects the recovery of the frozen shoulder patients.

It is reported that if rehabilitation exercises are transformed into interactive and entertaining games, patients will pay attention to the games and ignore the tedious training repetitions and pains during the rehabilitative exercises [CHY05, CZN05]. By interacting with VR gaming exercises, patients complete standard rehabilitation tasks natural [HKV02]. To design an interactive and effective rehabilitation environment for frozen shoulder patients, four common rehabilitative exercises should be included in design: flexion, abduction, internal rotation, and external rotation [MKP05]. Our proposed virtual reality

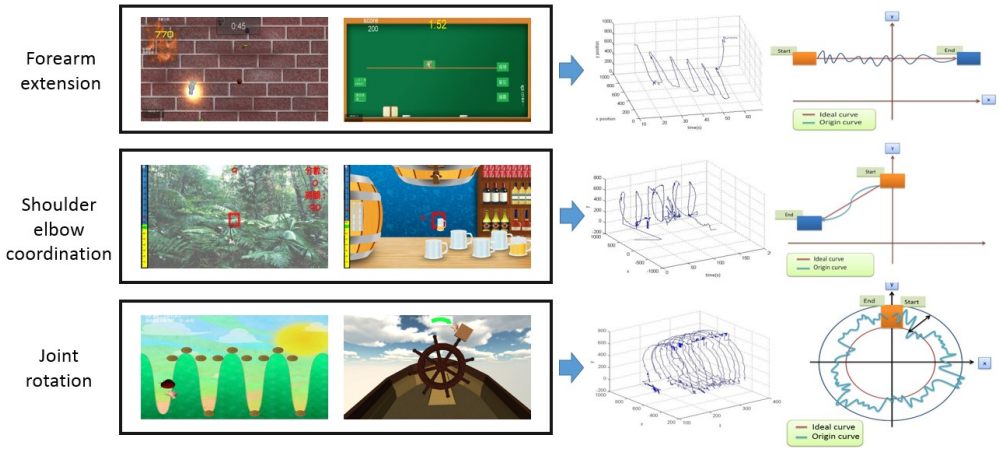

Figure 5.1: Six VR training tasks are grouped based on the rehabilitation targets. User motions are recorded as trajectories, projected onto 2D plane, and compared with the ideal path of the corresponding training task. Note that motion start is marked as a yellow box, end point is marked as a blue box, projected trajectories is indicated by a blue curve, and the ideal path is marked as a red curve.

(VR) game-based treatments fuses these important exercises together with muscle strength enhancement practices into three type of games: forearm extension training, shoulder-elbow interconnection training, and shoulder joint rotation training. Our study focuses on providing interactive treatments to encourage patients' participation and provides quantifiable monitoring and guiding system to assist physical therapists to track, design, and adjust training materials. The objective of this research is to combine virtual reality technology and wireless sensor technology to develop assessment instrument for self-measurement of the shoulder joint mobility and situated frozen shoulder rehabilitation system. Our real-time interaction and feedback design loyally presents the progress made by individual patients in real-time; therefore, patients can spontaneously inquiry their rehabilitation progress and understand their goals [KM67].

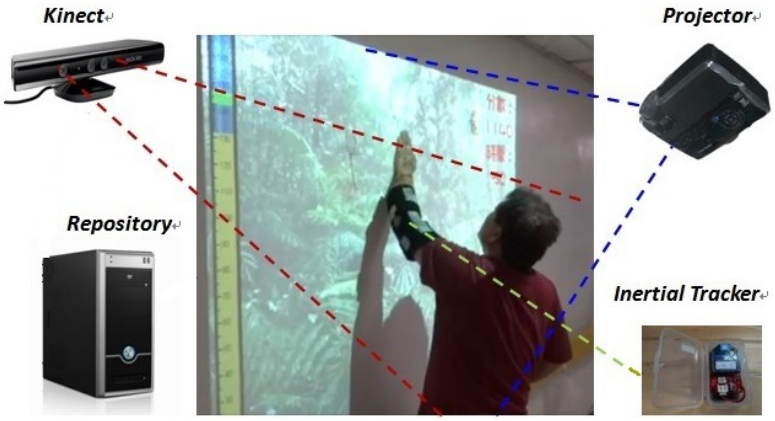

Figure 5.2: Virtual reality game-based training system

5.2 Frozen Shoulder Rehabilitation System

The system architecture is composed by VR game-based training task, real-time sensor system, and assisted daily objects. Patients are required to complete standard training tasks: flexion, abduction, external rotation, and internal rotation by interacting with designed VR rehabilitative training games. Six VR training tasks (Figure 5.1) are designed and categorize into three major exercises: forearm extension, shoulder elbow, and coordination, and joint rotation. Sensor system (Figure 5.2) collects patients' motion data during the game tasks by vision and inertial sensors. Collected data are stored in cloud repository for further analysis. Physical therapists can use this system to track, design, and adjust training materials for individual patients. In fact, each training step is adjustable based on patients' physical condition. For instance, a simple adjustment is to select an appropriate game level based on patients' current shoulder flexion and abduction condition. A patient is requested to face a wall and raise their hand to the highest height of the wall for estimating flexion. The same movement but the patient is requested to stand against to the wall on his/her side in the second time for estimating the shoulder abduction. Game level can be adjusted based on these initial measurements.

5.2.1 Forearm Extension

Two tasks are designed into this exercise mode to train the flexion and abduction ability of the patient. The first task is called Tracing. In this task, the patient has to link the targeted object on the left side of the screen to the object on the right with his/her palm of the affected shoulder. The trajectory from the left to the right may be horizontal, moving upward from the left and downward to the right, or moving downward from the left and moving upward to the right. The design allows the frozen shoulder patient to slowly stretch and extend his/her affected shoulder. The second task is called Reaching Fruit. In this task, the patient has to control a virtual palm in the task with his/her affected shoulder so as to reach all the fruits that appear continuously in the screen. This design allows the patient with frozen shoulder to lift his/her shoulder as high as possible and to stretch or extend the affected shoulder in the up, down, left, and right directions.

5.2.2 Shoulder-Elbow Exercise

Three games are designed in this exercise mode to enhance the flexion and abduction angles of the patient. In the beginning of the game, the patient is asked to lean his/her affected shoulder against a white wall, start stretching the affected shoulder, and hold for 10 seconds. Two of the tasks are related to Spiderman and Jungle Adventure. The player has to move his/her palm to the targeted object and as the player advances to a higher level of difficulty, he/she will need to lift his/her hand higher up in order to complete the task. The higher the level of difficulty, the more scores can be collected. The third game is called the Barman. The player controls the hand of a bartender in the virtual reality screen and has to complete tasks like taking the glass, filling it up, and placing it. The task allows the patient to stretch his/her affected arm against the white wall for 10 seconds.

5.2.3 Shoulder Joint Internal/External Rotation

Two games are designed in this exercise mode for stretching of the shoulder such as internal rotation, external rotation, and circumduction. The first task is called Ladybugs Game. In this task, the patient has to straighten his/her elbow to trace the motion trail of a ladybug. The second task is called Ship Driving. In this task, the patient is asked to straighten his/her elbow and turn the rudder clockwise or anti-clockwise for one full circle, as instructed.

5.2.4 Virtual Tutor

Real-time sensing technology further allow patients to watch their performance in real-time. Quantified progress results provides patient motivation to get better; therefore, patients are able to realize how much they have done and how much they should work on (Figure 5.3). Research showed that score feedback in VR can positively affect patients' motivation and have positive relationship with the improvement of disease [Cov, DeM07]. It is because that patient can actively involve in the self-measurement process and understand their body condition more. In addition the virtual tutor design let patients quickly examine themselves to see if they correctly follow the video guidance. Virtual tutor works as an mirror in front of the user, but it shows quantified numbers and visualizes the differences between the current progress and the desired goal. Video guidance and virtual tutor provides patients self-training capability. On the other hand, daily life objects, such as a tower and a wall, provide assisted functions to help patients complete game tasks without human intervention. Patients are learned to retain their body control with their own effort. Daily life objects, such as a tower and a wall, provide assisted functionality to help patients to complete game tasks. For instance, in Figure 5.2, a VR-game based training task is projected to a wall and guide a patient to exploit reacting counterforce from a wall to move their extrem-

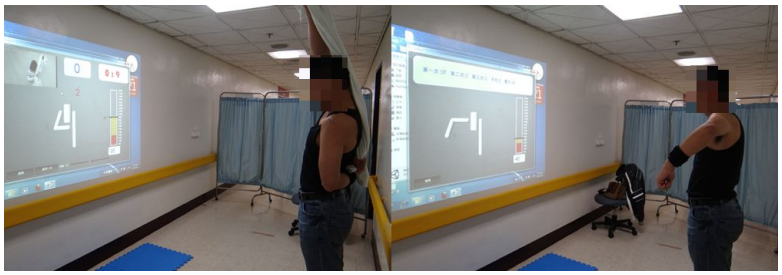

Figure 5.3: Video guidance and virtual tutor are used in the treatment process.

ities. As a result, they do not need any external assistance provided by therapists to stretch and rotate their joints of the extremities. Physical therapists merely need to demonstrate or tape the correct way to utilize common daily life object, such as stretching out a tower to play with ship driving game. Hence, Limited therapists are able to handle more suffered patients than before.

5.2.5 Real-time Interaction

Quantified data are collected from skeleton information of Microsoft Kinect. Acceleration and orientation data are from inertial sensors. User motions are recorded as time-indexed trajectories. Patients can immediately adjust their reaction based on the real-time fused kinematics feedback. Physical therapists can adjust gaming difficulties and design detailed parameters design based on the statistical analysis results. The analysis can provide them a quantifiable measurement for each patient's training and suggest a direction for future adjustment for individual patient. For example, some patients are suggested to use elastic ribbons to further enhance their muscle strength when they generate much of acceleration in manipulating virtual objects in the game scenes.

Table 5.1: Demographics of participants

	Study Group	Control Group
Case number	20	20
Average age	60.65 ± 11.84	61.45 ± 12.84
Male / Female	5/15	9/11
Course of disease (in month)	12.2 ± 6.2	10.4 ± 7.3

5.3 Evaluation

There were 40 patients with frozen shoulder problem were recruited for this prospective, interventional, randomized controlled, and single-blind study (Table 5.1). The experiment period is four weeks. Included subjects (1) were aged more than 20 years; (2) were never taken any physical therapy; (3) had frozen shoulder symptoms more than 3 months; and (4) were capable of participating in frozen shoulder rehabilitation based on VR. Patients were excluded from the study when they had (1) weakness or paralysis in the lower limbs; (2) current treatment with drugs for ototoxicity; (3) medical or surgical vestibular ablation treatment during the study period; or (4) cognitive dysfunction. Patients are randomly grouped into control and study groups following standard randomized clinical trials (RCT) criterion to evaluate the therapeutic effects and system feasibility. Each training tasks and the balance test were conducted and designed by a currently practicing licensed physical or occupational therapist.

Table 5.2: Shoulder joint angle test

Motion Angle	Pre-test			Post-test		
(Degree)	Study Group	Control Group	P-value	Study Group	Control Group	P-value
Flexion	149.1(129.2-162.7)	149.0(131.7-157.5)	.904	171.6 (153.2-174.0)	166.0(154.7-171.2)	*
Abduction	145.8(104.4-163.5)	144.0(100.7-163.9)	.947	168.0(1510.3-171.3)	157.7(127.7-169.9)	*
Externalrotation	62.1 (55.7-83.9)	60.0 (39.7-71.6)	.076	83.65 (71.5-88.2)	74.3 (56.5-81.2)	*
Internalrotation	40.5 (36.4-64.2)	37.1 (21.9-53.7)	.051	65.5 (54.0-71.9)	50.65 (40.2-59.0)	**
CMS assessment	63.5 (45.5-70.7)	63.0 (50.0-71.2)	.738	85.0 (72.5-89.0)	76.0 (68.2-84.7)	*

Significance Level = 0.05, *p-value ‘ 0.05, **p-value ‘ 0.01

Experiment procedures includes rehabilitation exercising training and hot pack and ultrasonic treatment [Car08]. All participants take hot pack and ultrasonic treatment to increase their muscle elasticity before they involve in the rehabilitative training. Patients are randomly selected as a member of study and control groups. Study group takes VR-based immersed training program and the control group takes traditional rehabilitation exercises. Both exercises are similar but members of study group have the privilege to receive real-time quantified motion feedback and VR game-based training. Full training program takes 20 minutes per visit and patients need to visit the rehabilitation center twice a week, 4 weeks in total. Study group patients are required to finish a series of rehabilitative exercise with/without physical objects, depending on the judgement made by the physical therapist. Sample motion tracking data are shown in Figure 5.1. The motion trajectories are extracted from the tracing game, barman, and ship driving. The rightmost plots present the 2D projection of the time-index trajectory data. T-wo boxes (colored with orange and blue) indicate the start and end point of the motion. Each game includes an ideal path which stands for the expected motion trajectory. The difference between the ideal path and the projected motion trajectory represents patients' gaming performance. To evaluate the affectivity of the VR system, patients of both study and control groups are evaluated with standard protractors by the authorized physical therapist. Both shoulders of freedom are tested with four basic exercises for every participants: flexion, abduction, internal rotation, and external rotation. Midspread estimation (interquartile range, IQR) of the joints angles analysis is performed and summarized in Table 5.2 to quantify the affectivity of VR-based and traditional rehabilitation methods. Members of the study group have 26% improvement after four weeks VR rehabilitative training, but members of the control group only have 18% improvement within the same four weeks period in general. In fact, the performance of the study group is outperformed than the control group in all four exercises. By examining the

pre-test data collected before the rehabilitation training, we can discover that the shoulder joints dexterity between the study and the control group is small. Patients in both groups has very similar capability in manipulating their shoulders. However, the result of the post-test of the study group reveals that patient's mobility of their shoulder joint are significantly improved than the control group treated with traditional rehabilitative method. Furthermore, subjects in the study group show high degree of technology acceptance and are willing to continue to use the proposed VR system for their rest of frozen shoulder rehabilitation.

5.4 Conclusion

Frozen shoulder or adhesive capsulitis, which is reported to affect 2% to 5% of the general population, describes the common shoulder condition characterized by painful and limited active and passive range of motion. Frozen shoulder patients in metropolitan area often dropped out their necessary rehabilitation according to our prior clinical experiences in Taipei Veteran General Hospital. One quarter of patients dropped out the standard treatment and rehabilitation processes because of their fast-pace and busy lifestyle. To overcome this situation, this study focuses on providing interactive treatments to encourage patients' participation in regular rehabilitation appointments. Patients can spontaneously inquire their rehabilitation progress with real-time sensing and game-based feedback. In addition, six progressive and hierarchical training tasks make each training step adjustable based on patients' physical condition. Forty patients were recruited for a sequence of trials within four weeks, following standard randomized clinical trials criterion. The evaluation of the study group reveals that patient's mobility of the shoulder joint and their muscle strength are significantly improved comparing with traditional rehabilitation method.

CHAPTER 6

Social Activity Promotion

6.1 Introduction

Research in many cultural settings has indicated that elderly people who choose to remain in their original homes and communities, despite their children living far away, often end up living alone [Cit11a]. Based on the U.S. Census in 2011, 29% of senior adults in the U.S. (8.1 million women and 3.2 million men) live alone [Cit11b]. A portion of this population gradually loses their connection with their families and friends because of isolated living situations and deteriorating social skills. A survey conducted by the Joseph Rowntree Foundation revealed that 19% of seniors in the U.K. who live alone communicate with their families on a face-to-face basis less than once a month [LXH13]. In addition, 17% of them are in contact with their families, friends, and neighbors less than once a week; instead, television becomes their main form of company [Bra13]. Gradually, these people lose their ability and willingness to communicate with others and often feel estranged and lonely for the remainder of their lives.

The fast pace of modern life further enlarges the gap between elderly people and the rest of society. They no longer remain informed about the world and express diminished enthusiasm for many former interests. Furthermore, the fast-paced lifestyles of younger generations results in having less time and patience for their parents and grandparents. BBC News [Cit05] reported that more than three million people feel disconnected from the modern life and isolated from society.

The lack of connection to the rest of the world affects people's health and can lead to severe mental illness, such as depression [Cit01]. Based on these facts, a social technology is introduced to assists elderly people in re-establishing communication with their families, old acquaintances, and making new friends.

Some researchers believe that a convenient interactive platform can help people to overcome their isolated living situations. They are encouraged to use the social technology to participate discussions of their living concerns with their peers and families [CZN05, PMP10]. Common topics of interest among elderly population are chronic diseases, personal life histories, and diet suggestions. Internet and wireless health technologies can provide health-related information, record and update personal and medical information, and offer remote health services to the community. Their daily activities and personal health conditions can be monitored, recorded, and summarized using cloud health care services; thus providing valuable health care information for personalized diagnosis. Their families can better understand the health and social conditions of their parents and obtain basic knowledge to help their parents. Nevertheless, medical information is so personal and private that most people do not like to share it openly. To address this privacy concern, Waycott et al. [Bat10] indicated that by sharing some daily photos and associated stories instead, elderly people can express themselves creatively and have regular communication with their friends as well. Nevertheless, it has been reported that some efforts to engage participants in the interests of their peers have been unsuccessful because of different life experiences.

Healthy diets and lifestyles can be another topic to be addressed [CGC12]. Because body composition and the health conditions of elderly people changes with age [FE73], they require nutrition information updates. Nevertheless, the process of searching nutrition information is time-consuming and often unstructured. In addition, requiring people to remember the food they consume daily and compare with their recommended intake is impractical because they are likely to forget and

confuse about what they have eaten. As a result, a system that enables people to log their dietary intake and look up nutrition information is necessary. The logged and cached nutrition information can be shared with other peers who have similar nutrition related concerns and with their families who are looking for help in caring for their parents.

Figure 6.1: FridgeNet implementation on a single fridge

FridgeNet (Figure 6.1) is designed for recording personal food intake information and promoting communication and social activity among senior citizens. The system employs sensor-equipped processing units (tablets mounted on standard refrigerators) and a cloud service to store and propagate food information. The system automatically stores users' dietary histories and downloads the corresponding nutrition information identified in the users' personal dietary histories. Similarly to existing social networking websites, the system enables users to post comments, pictures, and leave voice messages. The tablet-system also serves to propagate aggregated diet information among peers. Users can evaluate their nutrition intake by comparing their dietary history with other FridgeNet users. People can engage in FridgeNet social activities by regularly posting personal stories and subscribing food-consumption information within their online community. Furthermore, shared diet information can immediately assist those newcomers undergoing body condition changes during aging to adjust their diet styles.

6.2 Social Activity Promotion for Elderly People

Social activity has been a popular area of research since the introduction of social network media. A growing interest exists concerning the design and implementation of suitable social networks for aging populations as a means of reducing their experienced social isolation [DeM07, CHY05]. Some researchers have suggested that elderly people should participate in social networks to virtually connect with their families and friends, particularly if they live in isolated environments. For example, Burmeister et al. demonstrated that online communities can provide a space for elderly adults to share their life experiences and to create mutually supportive virtual communities. As elderly participants increase their online activities, they begin to value their participation in and contributions to a virtual community [Cov]. On the other hand, Bloch and Bruce observed an apparent disconnect between elderly people and their online participation. They suggest that additional research is required to determine enhancements to the online experience [Sec, LHS08]. For example, discovering a relevant topic may motivate people to use social network media spontaneously.

6.3 FridgeNet: Social Activity via Diet Sharing

FridgeNet is a prototype system consisting of multi-sensor-equipped tablets and a cloud-enabled application. This system is recommended for mounting on a standard refrigerator to monitor its changing content. User interactions with the refrigerator such as opening and closing actions are monitored by the system. Once an action is detected, users are prompted to input necessary information for daily dietary tracking, nutrition information retrieval, updated images, and social activity promotion (Buy2+gether). The following sections describe the individual functions of the FridgeNet related to diet monitoring and virtual social activity promotion.

6.3.1 Sensor-driven Interaction

Common inertial sensors are used on the tablet for automating the data recording process. When a user opens the fridge, the corresponding fluctuation is detected by the built-in accelerometer of the tablet. A prompt message is then triggered that instructs the user to scan a grocery receipt or select the food item name and take a picture to the food item taken out of the fridge. Both scanned receipt images and food snapshots are uploaded to the web service after recording. The item names on the receipt are recognized by an optical character recognition library [FH03] installed on the server-end. Information is processed by the FridgeNet software on the tablets and stored in the local database for periodic updating from the cloud server. An averaging peer diet intake information of every FridgeNet entity are accumulated in the cloud-end, so that each elderly participant can track their own diet habits and compare with this averaging truth from an elderly group daily. Therefore, a WiFi connection is required for each FridgeNet-enabled tablet. WiFi connectivity also provides FridgeNet location information. This information is used in the Buy2+gether service when a user enables the service and accepts invitations from peers.

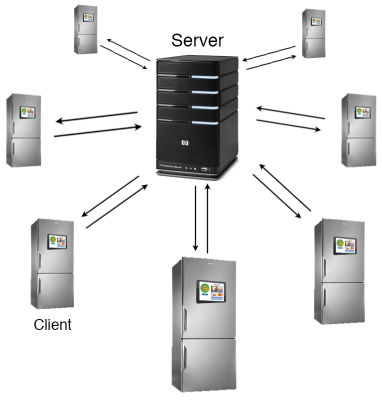

Figure 6.2: Client and server fridge network

6.3.2 Diet Tracking and Nutrition Analysis

Each food item on the receipt is tracked by FridgeNet. Users can browse the nutrition information of the tracked food through simple clicks on the tracked food list. If a food image is available, clicking on the image displays its nutrition information. Personal dietary history can be tracked and aggregated based on the history of receipt scanning. Consumed food is marked by users and recorded in the users' stored dietary history. Daily and weekly personal nutrition intake are calculated by accumulating the intake nutrition of all consumed food items. FridgeNet then periodically synchronizes individual dietary history, together with the cached nutrition information of newly added food, to the cloud server. The cloud end aggregates and calculates the average daily and weekly nutrition intake of the users. This summarized information is retrieved by FridgeNet when the next periodic update is issued by the cloud server.

6.3.3 Cloud Updates Visualization

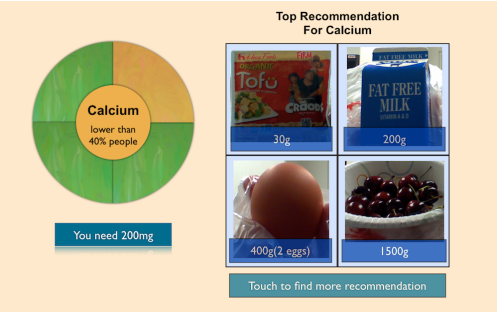

Figure 6.3: A sample nutrition comparison among peers

Figure 6.3 shows a donut chart that compares the differences in diets between the users and the peers. The chart is split into four sections representing four nutrition requirements for elderly people: iron, calcium, vitamin C, and vitamin D. When a user selects one of the four sections, the comparative results between the user and the peers are shown in the center and a pop-up notification appears

to indicate the amount the user requires. Each section of the donut chart is color coded based on the level of nutrition that the user requires, where green represents "sufficient", yellow represents "might be insufficient", and red represents "insufficient", and a user can quickly identify the nutrition component he or she lacks. This information is recalculated when an update from the server is retrieved by the FridgeNet tablet. On the right side of the donut chart, recommended foods for the user are displayed. The types of food recommendations are based on the pre-loaded and peer-recommended food types. The order of recommended food is sorted based on the amount of nutrition each item contains and the requirements for the user. For example, Figure 6.3 shows a hypothetical user who requires 200 mg or more of calcium in his or her daily diet. Thus, the most calcium-rich foods are listed and a recommended intake amount is provided below the food image. Users may click the button next to the image for more recommendations if the current suggestions are not preferred.

6.3.4 Food Recommendations and Response

Figure 6.4: The main page of the recommended food photo stream

Whenever a food item is removed from the refrigerator, a user is expected to mark the item name as consumed from the scanned receipt list and take a picture of that item. This action marks the food item as eaten and its nutrition informa-

tion is recorded in the user's daily log. If the food item is not fully consumed, the user should take another picture of the food item or simply input how much of the food remains. The current prototype assumes that all food contents inside the refrigerator were consumed by the elderly who lived alone and they are suggested to leave some messages if they share food with some visitors.

Users can selectively choose to provide comments on the food items they like. FridgeNet encourages and facilitates recommendations to peers. When users want to recommend a food item to peers, they can first press and hold the onscreen name or image of the item they want to recommend. A pop-up menu is displayed that confirms the recommendation. Users can optionally add text or voice messages to more adequately describe his or her recommendation. By contrast, if users discover that some recommended food is healthy, they can "like" the item (by pressing an indicator on the screen) or provide comments, and then place the food item in their virtual shopping cart. Figure 6.4 shows an example of a user who removed an apple from her refrigerator. Few minutes later, she leaves a comment saying she believes the apple is more delicious than the recommended food, cherries, even though cherries contain more vitamin C, as shown in the nutrient database.

6.3.5 Buy2+gether

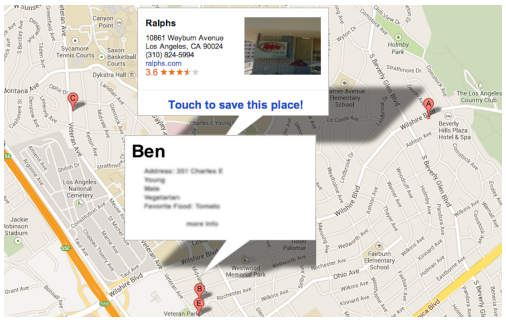

Figure 6.5: Buy2+gether application

FridgeNet is not only designed to promote virtual social interaction among

elderly people, but also to encourage elderly people to meet face to face. The Buy2+gether service (Figure 6.5) is an application that enables senior citizens to send shopping invitations to their neighbors to meet and purchase food together. Users can send shopping invitations based on the following criteria: 1) nutritional requirements, 2) the nearest three neighbors, or 3) an acquaintance (email address required), such as friends or family members. The person who initiates the shopping invitation can specify what he or she wants to buy, when to buy, and the deadline to accept the invitation. If invitations are accepted by the peers within the specified time frame, the participants can form a group and share contact information. FridgeNet helps to determine the most convenient location for the group to meet based on WiFi-positioning information, if requested. Figure 6.5 shows a FridgeNet suggestion for the most convenient grocery store for the group of participants.

6.4 Field Study

6.4.1 Participants

FridgeNet was evaluated with a group of 15 elderly people (10 women and 5 men) who lived alone and were between 55 and 76 years of age (AVG = 66.27, SD = 6.13). Some participants already knew other participants, but they did not regularly interact before the trial. Among the 15 participants, only five possessed experiences of using tablets for daily entertainment and none of them regularly used social networking media such as Facebook or Twitter. The families of the elderly participants also participated in the trial, although they were mainly observers and participated in a limited way during the study. They were allowed to access a FridgeNet website to see the general nutrition information and the aggregated diet information produced by participants. They were requested to observe rather than to join, except in the following two situations: 1) When a

senior family member had technical difficulty in using the FridgeNet system, and 2) When a senior family member sent Buy2+gether invitations to them.

6.4.2 Procedure

The whole study lasted 3 months. At the beginning of the experiment, every senior participant was taught how to use FridgeNet by the authors. To ensure safety, participants were recommended to consult with their personal doctors before changing their diet. Health effects associated with iron, calcium, vitamin C, and vitamin D deficiencies, as tracked by the FridgeNet prototype, were fully explained. They were then trained to scan their grocery receipts, photograph the food, read food nutrition information, respond with a "like" and provide comments and recommendations, and send invitations to specific groups of people. At least one family member of each elderly participant joined the training session. To encourage senior participants to use the Buy2+gether service, the authors suggested that families of the participants join in shopping events during the first month to help the senior participants to build confidence in meeting their peers. Participants were asked use the FridgeNet system to search for foods containing high percentages of calcium. Additional information about food nutrition was not provided in this study because it was expected that all participants would enjoy the process of determining nutrition requirements and locating that information in FridgeNet more than they would a lecture about nutrition.

6.4.3 Data Collection

Two types of data were collected during the experiment: FridgeNet data and questionnaire feedback. The following sections describe each type of data.

6.4.3.1 FridgeNet Data

Data from each FridgeNet entity were aggregated to the server (Figure 6.6). Each data stream included a unique ID. Researchers produced mapping tables to match unique IDs to the senior participants' personal information. This information was not accessible by participants nor family members. At the end of study, all tablets were collected to examine if any data was not correctly uploaded to the cloud servers and removed any of the participants' personal information on the tablets. FridgeNet collected food nutrition information and tablet usage log information such as the number of "likes" associated with a food item, comments, and Buy2+gether invitation messages.

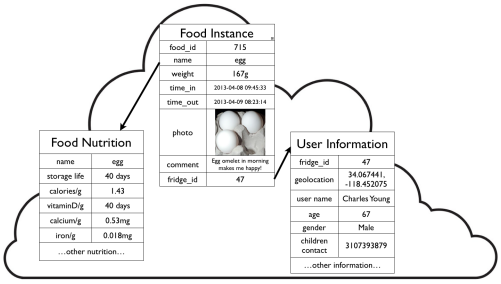

Figure 6.6: Food information is stored on a shared database for further analysis.

The primary statistical items used in the study were:

- Insufficient In-take Nutrition Statistics
- Click Rate of the Recommended Food
- Number of Comments and Feedback
- Number of Buy2+gether Invitation Replied

Data and an in-depth analysis are provided in the Results section.

6.4.3.2 Questionnaire

The elderly participants and their family members were asked to complete a questionnaire to provide feedback about their experiences. The participants rated their experiences base on a 9-point Likert scale, where 1 = strongly disagree, 3 = disagree, 5 = neither agree nor disagree, 7 = agree, and 9 = strongly agree. In addition, they were asked to answer a few open questions to suggest improvements to FridgeNet functionality. The questionnaire included the following items:

For Elderly Adults

(Q1) I feel I eat healthily.

(Q2) The system is easy to use.

(Q3) Reminding me what food is in the fridge is useful.

(Q4) I worry about privacy leaks concerning my eating habits.

(Q5) I am more willing to go outside.

(Q6) My children and I communicate more often.

(Q7) Open Question: It would be great if the system had this feature:

For Family Members

(Q1) I am learning about my parent's eating habits.

(Q2) My parent is in a good mood more often.

(Q3) I feel less anxious that they live alone.

(Q4) I will also use this system if you can provide a version for young adults.

(Q5) The message notification is disturbing.

(Q6) Open Question: It would be great if the system had this feature:

6.5 Results

This study attempts to answer three questions regarding the functionality of FridgeNet: 1) Does FridgeNet assist elderly people to choose healthy foods? 2) Does FridgeNet promote online social activities for participants? 3) Do the participants engage in more physical social activities after using FridgeNet than before using the system?

To answer the first question, statistics reveal the number of participants who had insufficient nutrition intake during the study period. To answer the second question, two categories of statistics are considered: a) the number of passive online activities the participant engages in, such as viewing food items or messages from peers, and the number of active online social activities the participant engages in, such as responding to peers recommendations with "likes" and personal comments. The last question is answered by determining the way in which Buy2+gether was used during the 12-week study. Each statistics analysis is discussed in the subsections below.

6.5.1 Insufficient Nutrition Intake Statistics

Analyzing nutrition intake trends is a method to determine whether FridgeNet improves elderly participant's food selection. Figure 6.7 presents the number of participants exhibiting insufficient nutrition intake in 12 weeks. Four major nutrition components for elderly people were tracked: iron (blue), calcium (green), vitamin C (yellow), and vitamin D (red). The figure shows that some of the participants exhibited lower levels of nutrition-intake sufficiency in the first week than did their peers on average. Eighteen insufficient-intake events were marked over 60 samples (15 participants x 4 tracked nutrition components). However, only 14 insufficient intake events were marked at the end of the study (51.7% improvement compared with the number in week 1). This phenomenon indicated

that the diet of the senior participants improved during the study period. One participant, a vegetarian, expressed that she never considered that she possesses insufficient levels of nutrition intake. She eats ample vegetable and fruits every day. However, by using this system, she realized that iron intake is commonly ignored by vegetarians. She quickly discovered that spinach, recommended by another vegetarian peer, could be appropriate for her. Furthermore, some of the participants said that they worried about insufficient nutrition and, therefore, required a system such as FridgeNet to determine their nutrition needs. Based on their feedback and nutrition-intake trends, this study determined that FridgeNet caused changes in the dietary behavior of those participants that possessed low levels of nutrition and was a catalyst for them to consider superior food choices.

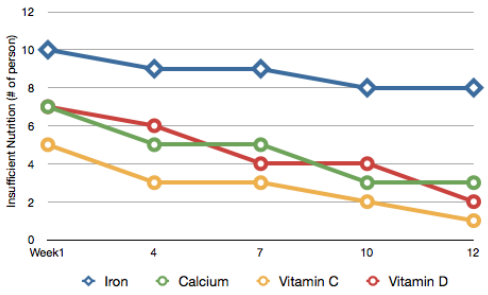

Figure 6.7: Four types of nutrition components which are commonly ignored by the elderly people in our study are presented. Most of participants learn to find out appropriate food for supplying the insufficient nutrition, but they seem to have difficulty in finding food with ample iron elements.

6.5.2 Click Number of the Recommended Food

Determining the number of clicks produced by each participant is an effective method to evaluate the frequency of FridgeNet use in the daily life of participants. Statistics on peer-recommended foods and the number of clicks associated with those foods are an indicator of levels of dietary improvement. Figure 6.8 shows that the participants made food recommendations to peers frequently. They pos-

sessed fewer privacy concerns regarding personal recommendations. Elderly participants recommended 47 foods in addition to the pre-loaded 50 food types. In addition, this study discovered that 76.3% of the recommended foods were selected more than once in the 12-week period. Popular foods such as apples were selected by all participants. In total, 1273 clicks occurred for all recommended foods in the course of the 12 weeks. On average, 7.07 clicks were produced per week by each person. Figure 6.8 presents the weekly average click counts of all 15 participants. Although some individuals produced more clicks than others, the click distribution shows that every participant used FridgeNet often to view peer recommendations. The analysis results revealed that the information obtained through FridgeNet was valuable to the senior community.

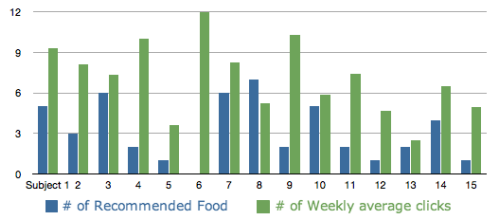

Figure 6.8: Numbers of recommended food by peers and the click number of the recommended food of all fifteen participants are presented. We can observe that most of participants check their peers' recommendation frequently and sometimes they recommend their favorite food to their peers.

6.5.3 Number of Likes and Comments

In addition to determining whether FridgeNet provides valuable information to elderly people, this study investigated whether FridgeNet promotes online social activities for elderly people. Specifically, this study attempted to determine whether FridgeNet encouraged them to acknowledge and comment during their online interactions with peers. First, the numbers of and trends associated with likes and comments were analyzed. The study was able to establish the frequency

with which senior participants participated in food-related discussions. Figure 6.9 revealed that the participants required approximately 2 weeks to familiarize themselves with the FridgeNet system. Only a few likes and comments were posted in the first week. The bulk of the comments and feedback started to appear during Week 3. In Week 3, 30 "likes" and 15 comments were posted. By Week 12, the number of likes tripled and comments doubled. This trend revealed that an increasing number of people were engaged in actively providing feedback. Even if they did not comment about a certain food type, they still participated by adding a like. Regarding the contents of comments, this study observed that certain food nutrition information was controversial For example, although spinach is said to contain abundant amounts of iron, many participants deemed it a potential cause of gall stones. Numerous discussions occurred about this concern and one participant stated that he read some articles online to contribute to the discussion. These observations demonstrated that FridgeNet encouraged people to share their knowledge and life experiences. Most elderly people in the study tended to be interested in and willing to join discussions.

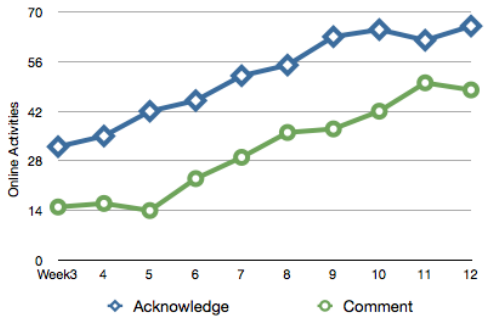

Figure 6.9: Numbers of feedback and comments leave in the FridgeNet system within 12 weeks. Although most people tends to 'like' the recommended food than leaves their comments, the increasing trend of both plots indicates that they become more active in participating FridgeNet online social activities.

6.5.4 Number of Replies to Buy2+gether Invitations

FridgeNet helped in building a virtual community focused on the topic of a healthy diet. It was also expected to promote physical social activities for elderly people by introducing the service, Buy2+gether. Unfortunately, only 11 shopping invitations were sent and only six were accepted during the 12-week study, indicating that this service was not used very often. Only seven events were recorded and the same group of four people were involved in these seven events. Figure 6.10 presented the people who participated in Buy2+gether service by Week 10. The shopping group originated with two senior adults, grew to three people by Week 7, and to five people by Week 10. The two group leaders were interviewed after Week 12 and stated that they preferred buying food with someone with whom they felt comfortable and that they selected friends based on replies to their recommendations rather than based on those who possessed similar food requirements. In fact, these two leaders knew each other because of the frequency with which they participated in online discussions about food. This demonstrates that online discussion about food nutrition can enhance understanding and familiarity among senior adults. These findings provide valuable information on the effect of the FridgeNet and Buy2+gether systems. Elderly people can more adequately use this system if frequent online interactions or regular social events occur that help them become familiar with their peers.

6.5.5 Questionnaire Statistics

Questionnaires were administered to both elderly people and their relatives. Their feedback enabled the evaluation of users subjective experiences related to multiple aspects of the system design and the studys effectiveness in promoting it. The analysis provided an enhanced understanding of user experience of the FridgeNet system.

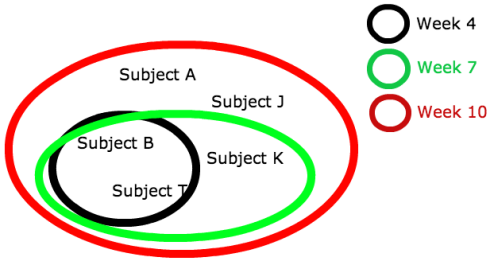

Figure 6.10: There are only five participants using Buy2+gether service withint 12 weeks. Subjects are marked as B, K, T, J, and A. We can observe that the same group of people uses this system and the group grows larger along with time. Black circle shows the initial group uses this service, Subject K joins later, and then Subject J and Subject A join. This indicates that Buy2+gether service is affective and attractive. Users have high loyalty in continuously using this service and are willing to recommend it to their friends.

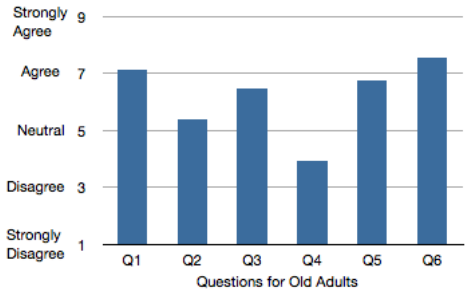

Figure 6.11: Old adults' averaging feedback

Figure 6.11 shows the average response from elderly participants. This study uses the t test for a population mean. This studys null hypothesis is $\mu = 5$, which means that, based on the studys participant feedback, the system is unlikely to produce a noticeably positive effect on users. This studys alternative hypothesis is $\mu>5$, which means the system will produce a noticeably positive effect on users. For Q4, because the sample mean is less than 5, this studys alternative hypothesis proves to be $\mu<5$. This study used 0.05 as the level of significance.

Q1 (AVG = 7.13, STDEV = 1.77, p = 1.838e-4) reflects the subjective experience

of nutrition promotion. This study demonstrated that the null hypothesis is rejected because of a low p value (<.05), which validates that FridgeNet promotes nutrition.

Q2 (AVG = 5.4, STDEV = 1.72, p = 1.915e-1) reflects the users experience in interacting with the FridgeNet system. This study demonstrated that the null hypothesis is not rejected because of a high p value (>.05), which indicates additional studies can improve user experience. The primary reason is that users must scan food every time they remove an item from the refrigerator.

Q4 (AVG = 3.93, STDEV = 1.49, p = 7.356e-3) reflects users' worries about privacy leaks. The null hypothesis is rejected, which indicates that users consent to this studys data collection.

Q5 (AVG = 6.73, STDEV = 1.83, p = 7.489e-5) rejects the null hypothesis and validates FridgeNet as effective in promoting outdoor activities.

Q6 (AVG = 7.53, STDEV = 1.77, p = 3.668e-5) rejects the null hypothesis and validates FridgeNet as effective in promoting family communication.

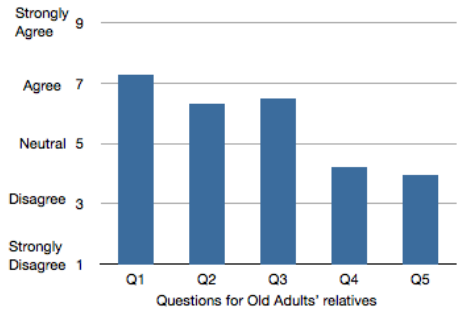

Figure 6.12: Old adults' relatives' averaging feedback

Figure 6.12 reveals the average response from relatives who receive daily nutrition summaries about their elderly relatives. This study uses the t test for a population mean. The null hypothesis, alternative hypothesis and significance level are the same as those for the elderly participant questionnaire, whereas Q5 and Q6 possess an alternative hypothesis μ<5.

Q1 (AVG = 7.27, STDEV = 1.67, p = 5.983e-5) indicates that FridgeNet successfully delivers required nutrition information to relatives of participants.
Q4 (AVG = 4.2, STDEV = 1.26, p = 1.378e-2) reflects that young people do not require a refrigerator to promote their social activities. This studys design focuses on the promotion of activity among elderly people who use the FridgeNet system.
Q5 (AVG = 3.93, STDEV = 1.83, p = 1.997e-2) indicates the daily summaries provided to relatives are helpful to understanding their parents' nutrition information.

6.6 Discussion: Nutrition Recommendation

Nutrition recommendations and discussions can be promoted either online or through physical activities. By sharing dietary habits and other comments and recommendations, elderly people in the study group learned to create and maintain a healthy lifestyle. FridgeNet provided a convenient framework, a popular topic for discussion, and a valuable healthy-diet database. Nevertheless, some limitations were revealed in the prototype. For example, although debatable nutrition information can be a topic for general discussion, a doctor's input is expected. One participant remarked, "I like discussion, but I love conclusion." The current FridgeNet community did not include medical or healthcare-related professionals. Therefore, if certain discussions contained errors or confusion regarding nutrition information, these may not have been corrected. A solution is to recruit certified medical professionals to monitor and participate in FridgeNet online discussions. Another approach is to encourage family members of participants to join discussions and provide professional references and articles about the discussed topics. For example, family members can send their elderly relatives monthly or quarterly reports to the medical professionals.

In addition, the system considers neither the different body types nor pre-existing conditions of participants, and it does not completely track the nutrition components of food. Users suggested that FridgeNet could include more intelligent grouping methods for recommending food based on different types of common illnesses and pre-existing conditions. In other words, FridgeNet may be able to provide a more reliable service by categorizing users into pre-defined groups. However, this strategy requires access to personal and medical information. Thus, a tradeoff is necessary in creating a system that offers comprehensive service and ensures privacy.

6.7 Discussion: Social Activity Promotion

FridgeNet not only promotes social activity among senior peers, it also reduces the distance between the elderly participants who live alone and their families. Both elderly participants and their families reported that voice messages were easy to produce through the FridgeNet system but more difficult to respond to regularly. Future research on how to convert voice messages to plain text may resolve this problem. Participants suggested that enabling FridgeNet to automatically schedule general activities could be an effective way to promote both virtual and physical activities among senior participants. Although this suggestion is considered, it should be noted that such a feature may reduce FridgeNet to a general social medium and cause it to lose its purpose as a health-specific tool for elderly people.

6.8 Conclusion

Social isolation among the elderly who live alone is an emerging social concern. A society in which elderly people have fewer offspring or have children who live

far away increases the number of people living alone. Inevitably, these isolated adults gradually lose their connection with society and their social skills worsen. FridgeNet is proposed to promote social activities for these people. By automating and encouraging the sharing of their diet information, mutual support in the virtual community is established. Continual communication and discussion further promote physical social activities such as groceries shopping with their peers. Based on the empirical results, this study concludes that FridgeNet is capable of increasing their social activities. 9 of 15 participants reported that they increased their interactions and received more attention from their families during the 3-month pilot study.

CHAPTER 7

Conclusion

This dissertation seeks new solutions to make medical resources, including medical facilities, medicine and professionals, accessible to anyone, anytime, anywhere. Technologies discussed should reduce medical costs, increase the engagement between patients and doctors, and promote inclusion and connectivity of individuals. Findings from this dissertation have the ability to make our healthcare system more effective and economic, which benefits both billions of individuals and the societies in which we live. My work not only develops complete solutions for innovative sensing and accurate analysis, but also leads to effective evaluation and actionable feedback design for the future healthcare field. Due to the completeness and interdisciplinary nature of my research, my research continually involves and benefits from researchers in a variety of research fields, such as public health, nursing, and behavioral science. I will further extend my research and collaboration to impact the development of the future medical and health services. Plenty of past studies have shown that the effectiveness of the medical treatment and intervention highly depends on the quality of patient compliance, such as whether taking medicine on time, doing exercise regularly, and having healthy food or not. My future research plan will work to understand patient behaviors, track their reactions with new sensing and interacting technologies, and explore new possibility of introducing technology into our everyday living.

My short-term future plan, three new potential healthcare applications are identified and debriefed below. Firstly, I plan to develop an unobtrusive sleep

quality monitoring system with continuous biophysical detectors to explore and quantify whether an appropriately designed environment can help people relax and have a good sleep. Furthermore, we can investigate whether people change their sleep patterns or behaviors (sleep postures, muscle pressure distribution, and breathing rhythms) along with environment changes and whether this knowledge can be exploited to promote better sleep habits. Secondly, designing eating pattern detection accessories, such as a fabric necklace, to remind people to eat healthy food and take medications on time. It can detect and record what is eaten, how much is eaten, and when does the eating event happen. The accessories should also support effective feedback methods, such as vibration or color changes to remind people to take appropriate actions in the right time. Last but not the least, I am interested in understanding human perception of surrounding atmosphere and comfortableness. By measuring biophysical signal changes on human bodies, we can explore whether human perception changes along with environmental changes. Specifically, we can investigate whether changing household environment can reduce people's feeling of high temperature and thus, eliminating unnecessary energy consumption.

References

[713] "Recommendations from COST 713 "UVB Forecasting"." www.who.int/uv/resources/recommendations/COST713.pdf.

[ATM01] H. Aoki, Y. Takemura, K. Mimura, and M. Nakajima. "Development of non-restrictive ensing system for sleeping person using fibre grating vision sensor." In *International Symposium on Micromechatronics and Human Science*, pp. 155–160. Nagoya, Japan, October 2001.

[Bat10] A. Bates. "Respiratory Rate and Flow Waveform Estimation from Tri-axial Accelerometer Data." In *Body Sensor Networks (BSN), 2010 International conference on*, pp. 144–150. IEEE press, 2010.

[Bed] Beddit. http://www.beddit.com/.

[Bil] Eli Billauer. "peakdet: Peak detection using MATLAB." http://www.billauer.co.il/peakdet.html.

[Bis06] Christopher Bishop. *Pattern Recognition and Machine Learning*. Springer, New York, 2006.

[Bjo67] Ake Bjorck. "Solving Linear Least Squares Problems by Gram-Schmidt Orthogonalization." *BIT Numerical Mathematics*, **7**(1):1–21, January 1967.

[Bla96] A. Blaugrund. "Notes on Doppler-Shift Lifetime Measurements." *Nuclear Physics*, **88**(3):501–512, November 1996.

[BLP09] O. Boric-Lukecke, V. Lubecke, B. Park, W. Massagram, and B. Jokanovic. "Heartbeat interval extraction using doppler radar for health monitoring." In *International Conference on Telecommunication in Modern Satellite, Cable, and Broadcasting Services*, pp. 139–142. Nis, Berbia, October 2009.

[Bor86] Gunilla Borgefors. "Distance transformations in digital images." *Computer vision, graphics, and image processing*, **34**(3):344–371, 1986.

[Bra13] Brian Brady. "Is this the loneliest generation? The Governmen-t is trying to quantify social isolation amid health fears.", 2013. http://www.independent.co.uk/life-style/health-and-families/health-news/is-this-the-loneliest-generation-8449305.html.

[BV04] S Boyd and L. Vandenberghe. *Convex Optimization*. Cambridge, New York, 2004.

[Car] Cardiac Direct. http://www.cardiacdirect.com/.

[Car08] J. Scott Cardozo. "New AASM Recommendations for Sensors: A Simple Guide for the Sleep Technologist." *Sleep Diagnosis and Therapy*, **21**(3), 2008.

[CBH08] M. Cretikos, R. Bellomo, K. Hillman, J. Chen, S. Finfer, and A. Flabouris. "Respiratory rate: the neglected vital sign." *Med J Aust*, **188**(11):657–659, 2008.

[CCH07a] M. Cretikos, J. Chen, K. Hillman, R. Bellomo, S. Finfer, and A. Flabouris. "The objective medical emergency team activation criteria: a case-control study." *Resuscitation*, **73**(1):62–72, 2007.

[CCH07b] M. Cretikos, J. Chen, K. Hillman, R. Bellomo, S. Finfer, and A. Flabouris. "The objective medical emergency team activation criteria: a case-control study." *Resuscitation*, **73**(1):62–72, January 2007.

[CGC12] Rob Comber, Eva Ganglbauer, Jaz Hee-jeong Choi, Jettie Hoonhout, Yvonne Rogers, Kenton O'Hara, and Julie Maitland. "Food and Interaction Design: Designing for Food in Everyday Life." In *CHI '12 Extended Abstracts on Human Factors in Computing Systems*, CHI EA '12, pp. 2767–2770, New York, NY, USA, 2012. ACM.

[CHY05] Yongjoon Chee, Jooman Han, Jaewoong Youn, and Kwangsuk Park. "Air mattress sensor system with balancing tube for unconstrained measurement of respiration and heart beat movements." *Physiological Measurement*, **26**(4):413, 2005.

[Cit01] "A phenomenological exploration of loneliness in the older adult." *US Department of Health and Human Services*, 2001.

[Cit05] "Busy lives leave elderly lonely.", 2005. `http://news.bbc.co.uk/2/hi/uk_news/4395477.stm`.

[Cit11a] "Global health and aging." *World Health Organization, National Institute on Aging, US Dept. of Health and Human Services*, 2011.

[Cit11b] "A profile of older Americans: 2011." *US Department of Health and Human Services*, 2011.

[CLL08] Mingqi Chen, O. Lubecke, and V. Lubecke. "0.5-um CMOS Implementation of Analog Heart-Rate Extraction With a Robust Peak Detector." *IEEE Transactions on Instrumentation and Measurement*, **57**(4):690–698, April 2008.

[CNK10] Yu Chi, Patrick Ng, Eric Kang, Joseph Kang, Jennifer Fang, and Gert Cauwenberghs. "Wireless non-contact cardiac and neural monitoring." In *ACM Conference on Wireless Health*, pp. 15–23. San Diego, October 2010.

[col] "Constitutive vs. Facultative Skin Color." `www.medscape.com/viewarticle/741045_2`.

[Cov] Covidien. "Nellcor Bedside Respiratory Patient Monitoring System." `http://www.covidien.com`.

[CRF05] Y. Chekmenev, H. Rara, and A. Farag. "Non-contact, wavelet-based measurement of vital signs using thermal imaging." In *ICGST International Conference on Graph, Vision and Image Processing*, pp. 25–30. Cairo, Egypt, December 2005.

[CRT06] Emmanuel Candes, Justin Romberg, and Terence Tao. "Stable Signal Recovery from Incomplete and Inaccurate Measurements." *Communications in Pure Applied Math*, **59**(4):1207–1223, April 2006.

[CZN05] Wenxi Chen, X Zhu, Tetsu Nemoto, Yumi Kanemitsu, Keiichiro Kitamura, and Ken-ichi Yamakoshi. "Unconstrained detection of respiration rhythm and pulse rate with one under-pillow sensor during sleep." *Medical and Biological Engineering and Computing*, **43**(2):306–312, 2005.

[DBG05] Ariel Diaz, Martial Bourassa, Marie Guertin, and Jean Tardif. "Long-term prognostic value of resting heart rate in patients with suspected or proven coronary artery disease." *European Heart Journal*, **26**(10):967–974, March 2005.

[DBL04] A. D. Droitcour, O. Boric-Lubecke, V. M. Lubecke, J. Lin, and G. T. A. Kovac. "Range correlation and I/Q performance benefits in single-chip silicon Doppler radars for noncontact cardiopulmonary monitoring." *IEEE Transactions on Microwave Theory and Techniques*, **52**(3):838–848, March 2004.

[DeM07] Susan DeMeulenaere. "Pulse Oximetry: Uses and Limitations." *The Journal for Nurse Practitioners*, **3**(5):312–7, 2007.

[DLL04] A. D. Droitcour, Olga Lubecke, Victor Lubecke, Jenshan Lin, and Gregory Kovacs. "Range correlation and I/Q performance benefits in single-chip silicon Doppler radars for noncontact cardiopulmonary monitoring." *IEEE Transactions on Microwave Theory and Techniques*, **52**(3):557–565, March 2004.

[Don04] D. Donoho. "Compressed Sensing." *IEEE Transactions on Information Theory*, **52**(4):1289–1306, April 2004.

[fac] "Skin Cancer Facts." `http://www.skincancer.org/skin-cancer-information/skin-cancer-facts`.

[FE73] Martin A. Fischler and R.A. Elschlager. "The Representation and Matching of Pictorial Structures." *Computers, IEEE Transactions on*, **C-22**(1):67–92, 1973.

[FH03] Pedro F. Felzenszwalb and Daniel P. Huttenlocher. "Pictorial Structures for Object Recognition." *IJCV*, **61**:2005, 2003.

[FH09] R. Fletcher and J. Han. "Low-cost differential front-end for Doppler radar vital sign monitoring." In *International Microwave Symposium Digest*, pp. 7–12. Boston, USA, June 2009.

[FHH93] JF. Fieselmann, MS. Hendryx, CM. Helms, and DS. Wakefield. "Respiratory rate predicts cardiopulmonary arrest for internal medicine patients." *J Gen Intern Med*, **8**(7):354–360, 1993.

[For] ForaCare. `http://www.foracare.com/`.

[FPF99] Andrew Fitzgibbon, Maurizio Pilu, and Robert Fisher. "Direct Least Square Fitting of Ellipses." *IEEE Transactions on Pattern Recognition and Machine Intelligence*, **21**(5):476–480, May 1999.

[FYP13] M. Farshbaf, R. Yousefi, M. Baran Pouyan, S. Ostadabbas, M. Nourani, and M. Pompeo. "Detecting high-risk regions for pressure ulcer risk assessment." In *International Conference on Bioinformatics and Biomedicine.* IEEE press, 2013.

[GIL] C. Gu, T. Inoue, and C. Li. "Analysis and Experiment on the Modulation Sensitivity of Doppler Radar Vibration Measurement." In *IEEE Microwave and Wireless Components Letters*, p. in print.

[GLF12] C. Gu, R. Li, R. Fung, C. Torres, S. Jiang, , and C. Li. "Accurate Respiration Measurement using DC-Coupled Continuous-Wave Radar Sensor for Motion-adaptive Cancer Radiotherapy." *IEEE Transactions on Biomedical Engineering*, **59**(11):3117–3123, November 2012.

[GSH11] R. Grimm, J. Sukkau, J. Hornegger, and G. Greiner. "Automatic patient pose estimation using pressure sensing mattresses." In *Bild-verarbeitung fur die Medizin.* ser. Informatik aktuell, 2011.

[GWC97] A. Groote, M. Wantier, G. Cheron, M. Estenne, and M. Paiva. "Chest Wall Motion During Tidal Breathing." *Journal of Applied Physiology*, **83**(1):1531–1537, June 1997.

[HC11] G. Hughes and M. Chraibi. "Calculating ellipse overlap areas." *ArXiv eprints 1106.37.87*, pp. 1–49, 2011.

[HF98] Radim Halir and Jan Flusser. "Numerically Stable Direct Least Squares Fitting Of Ellipses.", 1998.

[HFW03] Tamara Salam Housman, Steven R Feldman, Phillip M Williford, Alan B Fleischer Jr, Neal D Goldman, Jose M Acostamadiedo, and G John Chen. "Skin cancer is among the most costly of all cancers to treat for the Medicare population." *Journal of the American Academy of Dermatology*, **48**(3):425–429, 2003.

[HGR94] Ellen Herlihy, Peter H Gies, Colin R Roy, and Michael Jones. "Personal dosimetry of solar UV radiation for different outdoor activities." *Photochemistry and photobiology*, **60**(3):288–294, 1994.

[HKV02] Timothy J Hodgetts, Gary Kenward, Ioannis G Vlachonikolis, Susan Payne, and Nicolas Castle. "The identification of risk factors for cardiac arrest and formulation of activation criteria to alert a medical emergency team." *Resuscitation*, **54**(2):125–131, 2002.

[HMC04] Shasa Hu, Fangchao Ma, Fernando Collado-Mesa, and Robert S Kirsner. "UV radiation, latitude, and melanoma in US Hispanics and blacks." *Archives of dermatology*, **140**(7):819, 2004.

[HS10] David Heise and Marjorie Skubic. "Monitoring pulse and respiration with a non-invasive hydraulic bed sensor." In *Conf Proc IEEE Eng Med Biol Soc*, pp. 2119–23, 20010.

[HTW10] A. Hart, K. Tallevi, D. Wickland, R.E. Kearney, and J.A. Cafazzo. "A contact-free respiration monitor for smart bed and ambulatory monitoring applications." In *Engineering in Medicine and Biology Society (EMBC), 2010 Annual International Conference of the IEEE*, pp. 927–930, 2010.

[KKW64] E. Kinnen, W. Kubicek, D. Witsoe, R. Patterson, and USAF School of Aerospace Medicine. *Thoracic Cage Impedance Measurements: Impedance Plethysmographic Determination of Cardiac Output (an Interactive Study)*. Technical documentary report, SAM-TDR. USAF School of Aerospace Medicine - Aerospace Medical Division (AFSC), 1964.

[KM67] K. Konno and J. Mead. "Measurement of the separate volume changes of rib cage and abdomen during breathing." *Journal of Applied Physiology*, **22**(3):407–422, 1967.

[Lee95] V Leenutaphong. "Relationship between skin color and cutaneous response to ultraviolet radiation in Thai." *Photodermatology, Photoimmunology & Photomedicine*, **11**(5-6):198–203, 1995.

[LHS08] Siân E. Lindley, Richard Harper, and Abigail Sellen. "Designing for Elders: Exploring the Complexity of Relationships in Later Life." In *Proceedings of the 22Nd British HCI Group Annual Conference on People and Computers: Culture, Creativity, Interaction - Volume 1*, BCS-HCI '08, pp. 77–86, Swinton, UK, UK, 2008. British Computer Society.

[Lik32] Rensis Likert. "A technique for the measurement of attitudes." *Archives of psychology*, 1932.

[Lin92] J.C. Lin. "Microwave sensing of physiological movement and volume changes: a review." *Bioelectromagnetics*, **13**(3):557–565, November 1992.

[LL08] Changzhi Li and Jenshan Lin. "Random Body Movement Cancellation in Doppler Radar Vital Sign Detection." *IEEE Transactions on Microwave Theory and Techniques*, **56**(12):3143–3152, December 2008.

[LXH13] J. Liu, W. Xu, MC. Huang, N. Alshurafa, and M. Sarrafzadeh. "A Dense Pressure Sensitive Bedsheet Design for Unobtrusive Sleep Posture Monitoring." In *Pervasive Computing and Communications (PerCom), IEEE Int. Conf.* IEEE press, 2013.

[LYK11] Choonghee Lee, Chiyul Yoon, H. Kong, Hee Chan Kim, and Youngwook Kim. "Heart Rate Tracking Using a Doppler Radar With the Reassigned Joint Time-Frequency Transform." *IEEE Antennas and Wirelss Propagation Letters*, **10**(5):1096–1099, May 2011.

[met] "Solartech Inc." `http://www.solarmeter.com/modelPUVM.html`.

[MKP05] Jackie McBride, Debbie Knight, Jo Piper, and Gary B Smith. "Long-term effect of introducing an early warning score on respiratory rate charting on general wards." *Resuscitation*, **65**(1):41 – 44, 2005.

[MLM09] W. Massagram, V. Lubecke, A. Madsen, and O. Boric-Lubecke. "Assessment of Heart Rate Variability and Respiratory Sinus Arrhythmia via Doppler Radar." *IEEE Transactions on Microwave Theory and Techniques*, **57**(10):2542–2549, October 2009.

[MPT04] R. Murthy, I. Pavlidis, and P. Tsiamyrtzis. "Touchless monitoring of breathing function." In *Annual International Conference of the IEEE Engineering in Medicine and Biology Society*, 2004.

[NMW11] M. Nishyama, M. Miyamoto, and K. Watanabe. "Respiration and body movement analysis during sleep in bed using hetero-core fiber optic pressure sensors without constraint to human activity." *Journal of Biomedical Optics*, **16**(1):017002–017002–7, 2011.

[Omr] Omron Inc. `http://www.omronhealthcare.com/`.

[Phi] Philips. "Vital Signs Camera." `http://www.vitalsignscamera.com`.

[PKO03] MA. Peberdy, W. Kaye, JP. Ornato, GL. Larkin, V. Nadkarni, ME. Mancini, RA. Berg, G. Nichol, and T. Lane-Trultt. "Cardiopulmonary resuscitation of adults in the hospital: a report of 14720 cardiac arrests from the National Registry of Cardiopulmonary Resuscitation." *Resuscitation*, **58**(3):297–308, 2003.

[PLL07] B. Park, O. Lubecke, and V. Lubecke. "Arctangent Demodulation With DC Offset Compensation in Quadrature Doppler Radar Receiver Systems." *IEEE Transactions on Microwave Theory and Techniques*, **55**(5):1073–1079, May 2007.

[PMP10] Ming-Zher Poh, Daniel J. McDuff, and Rosalind W. Picard. "Non-contact, automated cardiac pulse measurements using video imaging and blind source separation." *Optics Express*, **18**, 2010.

[PYL07] B. Park, S. Yamada, and V. Lubecke. "Measurement Method for Imbalance Factors in Direct-Conversion Quadrature Radar Systems." *IEEE Microwave and Wirelss Components Letters*, **17**(5):403–405, May 2007.

[RM11] Kristin Reed and Rick May. "HealthGrades Seventh Annual Patient Safety in American Hospitals Study." *HealthGrades, Inc.*, 2011.

[Rob05] June K Robinson. "Sun exposure, sun protection, and vitamin D." *JAMA: the journal of the American Medical Association*, **294**(12):1541–1543, 2005.

[RS89] G. Ramachandran and M. Singh. "Three-dimensional reconstruction of cardiac displacement patterns on the chest wall during the P, QRS, and T-segments of the ECG by laser speckle interferometry." *Medical Bioengineering Computing*, **27**(1):525–530, June 1989.

[RW06] C. Rasmussen and K. Williams. *Gaussian Processes for Machine Learning*. MIT Press, Cambridge, MA, USA, 2006.

[RWH10] Howard W Rogers, Martin A Weinstock, Ashlynne R Harris, Michael R Hinckley, Steven R Feldman, Alan B Fleischer, and Brett M Coldiron. "Incidence estimate of nonmelanoma skin cancer in the United States, 2006." *Archives of dermatology*, **146**(3):283, 2010.

[RXS10] M. Rofouei, Wenyao Xu, and M. Sarrafzadeh. "Computing with uncertainty in a smart textile surface for object recognition." In *Multisensor Fusion and Integration for Intelligent Systems (MFI), 2010 IEEE Conference on*, pp. 174–179, Sept 2010.

[SCH12] Zygmunt Szpak, Wojciech Chojnachi, and Anton Hegel. "Guaranteed Ellipse Fitting with the Sampson Distance." In *12th European Conference on Computer Vision*, pp. 18–23. Firenze, Italy, October 2012.

[Sec] SecuraTrac. "SecuraFone Health." `http://www.securafone.com/subpages/health.php`.

[tan] "Skin cancer - tanning." `http://www.betterhealth.vic.gov.au/bhcv2/bhcarticles.nsf/pages/Skin_cancer_tanning?open`.

[TLW09] Y. Tao, J. Long, J. Wang, W. Cui, W. Ma, J. Huangfu, and L. Ran. "A Novel Non-contact Vital Sign Detection System Based on Phase-Coded Pulse Radar." In *IET Conference on Wireless Mobile and Computing*, pp. 421–424. Hangzhou, China, December 2009.

[VP04] Emil Valchinov and Nicolas Pallikarakis. "An active electrode for biopotential recording from small localized bio-sources." *BioMedical Engineering OnLine*, **3**(1):25, 2004.

[WEM90] Wiete Westerhof, Oscar Estevez-Uscanga, Joes Meens, Arthur Kammeyer, Muriel Durocq, and Irina Cario. "The relation between constitutional skin color and photosensitivity estimated from UV-induced erythema and

pigmentation dose-response curves." *Journal of investigative dermatology*, **94**(6):812–816, 1990.

[wri] "The disposable wristband that can tell you when to get out of the sun." `http://www.dailymail.co.uk/sciencetech/article-2186003/`.

[WWT05] K. Watanabe, T. Watanabe, H Tatanabe, H. Ando, and T. Ishikawa. "Non-invasive measurement of heartbeat, respiration, snoring and body movements of a subject in bed via a pneumatic method." *IEEE Transactions on Biomedical Engineering*, **52**(12):2100–2107, December 2005.

[WYG09] J. Wright, Y. Yang, A. Ganesh, S. Sastry, and Y. Ma. "Robust Face Recognition via Sparse Representation." *IEEE Transactions on Pattern Recognition and Machine Intelligence*, **31**(2):210–227, Feb. 2009.

[XGL12] W. Xu, C. Gu, C. Li, and M. Sarrafzadeh. "Robust Doppler radar demodulation via compressed sensing." *Electronics Letters*, **48**(22):1428–1430, 2012.

[XLH11] W. Xu, Z. Li, MC. Huang, N. Amini, and M. Sarrafzadeh. "ecushion: an etextil device for sitting posture monitoring." In *Body Sensor Networks (BSN), 2011 International conference on*, pp. 194–199. IEEE press, 2011.

[XZS12] W. Xu, M. Zhang, A. Sawchuk, and M. Sarrafzadeh. "Robust Human Activity and Sensor Location Co-Recognition via Sparse Signal Representation." *IEEE Transactions on Biomedical Engineering*, **58**(11):1–10, Nov. 2012.

[ZFP05] Z. Zhu, J. Fei, and I. Pavlidis. "Tracking Humane Breath in Infrared Imaging." In *IEEE Symposium on Bioinformatics and Bioengineering*, pp. 227–231. Washington DC, July 2005.

[ZH05] Z. Zhu and X. Huang. "Bias Analysis of A Gain/Phase/DC-offset Estimation Technique for Direct Frequency Conversion Modulators." In *IEEE International Conference on Acoustics, Speech, Signal Processing*, pp. 18–23. Ottawa, Canada, March 2005.

[ZRV12] M. Zakrzewski, H. Raittinen, and J. Vanhala. "Comparison of Center Estimation Algorithms for Heart and Respiration Monitoring With Microwave Doppler Radar." *IEEE Sensors Journal*, **12**(3):627–634, March 2012.